Estimates of Water Turbine Noise Levels

by

Julian Guerra

A Thesis Submitted to the Faculty of

The College of Engineering and Computer Science

in Partial Fulfillment of the Requirements for the Degree of

Master of Science

Florida Atlantic University

Boca Raton, Florida

May 2011

Estimates of Water Turbine Noise Levels

by

Julian Guerra

This thesis was prepared under the direction of the candidate's thesis advisor, Dr. Stewart Glegg, Department of Ocean and Mechanical Engineering, and has been approved by the members of his supervisory committee. It was submitted to the faculty of the College of Engineering and Computer Science and was accepted in partial fulfillment of the requirements for the degree of Master of Science.
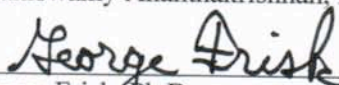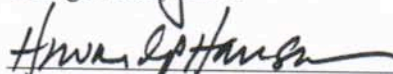
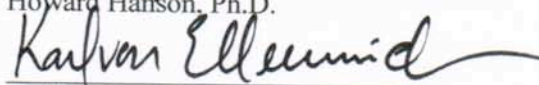SUPERVISORY COMMITTEE:

Stewart Glegg, Ph.D.
Thesis Advisor
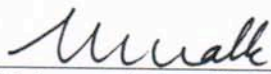
Palaniswamy Ananthakrishnan, Ph.D.
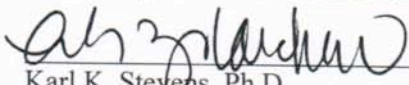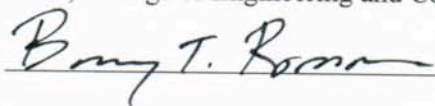
George Frisk, Ph.D.

Howard Hanson, Ph.D.

Karl D. von Ellenrieder, Ph.D.

Mohammad Ilyas, Ph.D.
Chair, Department of Ocean and Mechanical Engineering

Karl K. Stevens, Ph.D.
Dean, College of Engineering and Computer Science

Barry T. Rosson, Ph.D. Dean, Graduate College

April 14, 2011

Date

ii

Abstract

Author: Julian Guerra

Title: Estimates of Water Turbine Noise Levels

Institution: Florida Atlantic University

Thesis Advisor: Dr. Stewart Glegg

Degree: Master of Science

Year: 2011

This work seeks to understand water turbine noise generation and to make preliminary estimations of the noise levels. Any structure attached to a turbine upstream its blades will generate unsteady fluctuating loads on the blade's surface, which are proportional to the radiated acoustic pressure. The noise levels of a simplified turbine based on existing designs surpass the ambient noise levels of the ocean at low frequencies (< 20 Hz) by approximately 50 dB ref 1 µPa, and stay under the ambient noise levels at higher frequencies for a blade-passing frequency of 0.83 Hz and point of observation (100 m, 45º, 45º) from the hub. Streamlining the cross-section of the upstream structure as well as reducing its width decrease the noise levels by approximately 40 dB ref 1 µPa, at low frequencies and moderately increase them at higher frequencies. Increasing the structure-rotor distance decreases the noise levels with increasing frequencies (> 30 Hz).

Estimates of Water Turbine Noise Levels

List of Tables

List of Figures

ix

Chapter 1: Introduction

1.1 Overall objective

In recent years there has been a need for alternative, cleaner and more efficient ways to produce energy and one method currently proposed is harnessing power from ocean currents by utilizing hydrokinetic turbines. However, one of the concerns with this technology is the impact that the turbine noise will have on the marine environment. Therefore, the intent of this project is to provide a description of the physical mechanisms behind the generation of water turbine noise and to develop a mathematical model that will provide estimates of the noise levels. These estimates can then be used to assess the environmental impact of water turbine noise as well as to provide an insight into what improvements can be made to existing turbine designs to reduce the noise levels.

1.2 Approach

The noise from water turbines is expected to be similar to the noise from wind turbines and marine propellers, it is well known that wind turbines and propellers produce two types of acoustic signatures, namely, harmonic noise and broadband noise. The relative importance of these two acoustic signatures for hydrokinetic turbines is yet to be determined and will not be possible until base line measurements are taken. Thus, this work will focus on the harmonic noise, specifically on the harmonic noise generated by velocity deficit profiles formed upstream of the blades.

From studies on wind turbines, it is expected that the upstream structure supporting the rotor will create disturbances to the inflow velocity, which will cause fluctuating loads on the blades. Similarly, the water turbine design that will be studied here has an upstream structure supporting two buoyancy modules, causing a loading fluctuating on the turbine blades. An important point to be made at this point is that this study will only be concerned with the harmonic noise generated by velocity deficit profiles formed upstream of the blades and will leave the unsteady loading noise created by vortex shedding off the structure, known as blade vortex interaction (BVI) to be considered as a topic of study for future works.

The Ffowcs Williams and Hawkings equation, which describes the acoustic pressure field generated by a surface moving in an otherwise stationary fluid relate the load fluctuations on the blade to the noise radiation. Also, it is expected that due to the characteristics of the water turbine, the Ffowcs Williams and Hawkings equation will be reduced to only one term known as the dipole term, which depends on the loading fluctuations on the blade. These loading fluctuations can be decomposed into a drag fluctuation and a lift fluctuation component, which can occur either in a steady or unsteady manner. Both steady and unsteady fluctuations are expected to occur in water turbines, but it is expected from studies in non-cavitating propellers that the unsteady lift fluctuations will be the dominant source of noise for water turbines. The unsteady lift on the blades can be obtained by using Sears's theory for two-dimensional thin airfoils passing through a vertical gust pattern having a sinusoidal distribution of unsteady velocity. The two-dimensional assumption will be justified by the fact that the water turbine design has a high aspect ratio, which simplifies some of the calculations by the

implementation of strip theory. The expression of the unsteady lift based on Sear's theory depends on a vertical velocity perturbation felt on the blades, which is known as the upwash velocity. The upwash velocity is a byproduct of changes in the angle of attack, which are generated by incoming velocity disturbances originated at the structure upstream of the blades. The incoming velocity disturbances will be modeled by using Wygnanski, Champagne and Marasli's theory for a two-dimensional, turbulent, small-deficit wake. This theory yields an expression of the velocity profile downstream of a structure, which will then be used to derive an expression for the upwash velocity by considering the interacting velocities affecting the blade. Sear's expression of the lift calls for the Fourier coefficients of the upwash velocity, which are calculated by taking advantage of the periodicity of the blade motion.

Once the expressions for the upwash velocity and the time derivative of the unsteady lift are derived, the dipole term in the FW-H equation will be used to estimate the radiated noise levels. This equation, however, presents a difficulty because its results are given in observer's time, which differs from the emission time used in the derivation of the unsteady lift expression. Thus an interpolation method will be applied to the FW-H equation in order to solve this time delay problem. To obtain the noise levels, it will first be necessary to get an expression for the time history of the acoustic field and then to calculate the frequency spectrum from this signal. Finally, the power spectrum is presented on a decibel scale and corrected for the transmission losses to obtain the effective source levels. These results will be used to make an assessment of water turbine noise and it's impact on the marine environment. Also, an analysis will be given of the changes to the water turbine design that will help to reduce the noise levels.

1.3 Summary of Each Chapter

Chapter 2 presents a summary on the studies of wind turbines and marine propeller noise generation. This chapter also introduces the concepts of acoustic analogy, the Ffowcs Williams and Hawkings equation, loading noise and forces due to a sinusoidal gust. Chapter 3 gives a full description of all the characteristics of the turbine design studied here, and Chapter 4 presents the application of the acoustic analogy to the water turbine noise problem as well as the description of the simplifications and assumptions made in the derivation of the loading noise equation. This chapter also introduces the interpolation methods that will be applied to the time histories of the acoustic field. Chapter 5 deals with the mechanisms of the unsteady lift and the mathematical model that describes it. This chapter also introduces the concept of upwash gust velocity. Chapter 6 describes the physical mechanisms and the mathematical model of the upwash velocity generated by the velocity profile behind the structure. In chapter 7, all the all the results are combined to the yield an expression for the radiated acoustic pressure. Also, expressions for the average power and source levels are obtained. In chapter 8, alternative designs of the turbine are considered and their noise levels are estimated. These results are obtained by changing three different parameters of the original design; shape and width of the upstream structure and the distance between the blade and the structure, the results are fully discussed and compared to ocean's ambient noise levels. Finally, chapter 9 presents the conclusions and final discussion of the results and methods used in this investigation.

Chapter 2: Literature Review

2.1 Wind Turbine Noise

It is well known that wind turbine noise is a combination of aerodynamic noise generated by the blades and mechanical noise [1]. Insulating the nacelle or tower in order to attenuate noise can efficiently reduce mechanical noise, which is caused by the turbine's internal gears. Aerodynamic noise on the other hand is generated by the blades passing through the air and is more complex and difficult to eliminate [1]. The sound power of aerodynamic noise is related to the ratio of the blade tip to the wind speed, causing different effects depending on the size and model of the turbine [1]. Among these effects are: the "wa-wa" oscillations generated by the so-called wind park effect (effects of a turbine on its neighbors in a wind turbine farm) and the thumping sound created by turbines with their blades downwind of the tower.

Also, the aerodynamic noise produced by wind turbines can be non-periodic, producing an acoustic signature known as broadband noise. Different types of sources, such as, tip noise, inflow turbulence noise, blunt trailing-edge noise or turbulent boundary-layer trailing-edge interaction noise, can cause this broadband noise [1]. The thumping effect is expected to occur in existing designs of water turbines, since their blades are located downstream of a structure supporting two buoyancy modules. However, for water turbines, the importance of the broadband signature has not yet been

determined, and it will not be possible to estimate this until base line measurements of water turbine noise are taken.

2.2 Marine Propeller Noise

There are four types of noise that can be produced by a propeller; displacement noise, which is due to the water displaced by the rotating blade; fluctuation load noise, which is caused by non-uniformities in the incoming flow causing unsteady blade loading; cavity noise caused by periodic fluctuation of the cavity volumes in the wake behind the marine vehicle and cavitation noise caused by the sudden collapse process associated with cavitation bubbles [2]. These sources can be divided into cavitating and non-cavitating components, with the first two being non-cavitating and the latter two being caused by cavitation. Cavitating propeller noise is only important for propellers operating near the surface while non-cavitating propeller noise dominates when the propeller operates at depths where cavitation is avoided. For the case of water turbines, which will initially be deployed at a depth of approximately 10 m, their cavitation number is.

$$\sigma_o = \frac{P_o - P_v}{\frac{1}{2}\rho U_{tip}^2} \approx \frac{202000 - 2500}{\frac{1}{2}(1023)(7.85)} \approx 6.32$$

Where

P_o = is a characteristic pressure level

P_v = vapor pressure

U_{tip} = is the tip velocity of the blade roughly calculated using tip speed ratio TPR = 4.62 [3].

Cavitation occurs for $\sigma_o = 0.1$ or less.

2.3 The Acoustic Analogy

The Ffowcs Williams and Hawkings wave equation gives a method to calculate the sound generated rotating blades in an otherwise stationary fluid, and is given as [4]

$$\frac{1}{c_o}\frac{\partial p'}{\partial t^2} - \nabla^2 p' = \frac{\partial}{\partial t}\left[\rho v_n \mid \nabla f \mid \delta(f)\right] - \frac{\partial}{\partial x_i}\left[F_i \mid \nabla f \mid \delta(f)\right] - \frac{\partial^2}{\partial x_i \partial x_j}\left[T_{ij}H(f)\right] \quad (1)$$

Where

$f = 0$ on the surface of the blade

n_j = surface normal outward (f=0)

p' = acoustic pressure

c_o =speed of sound

ρ = Mean fluid density

v_n = local normal velocity (blade surface)

F_i = force per unit area applied on the fluid

T_{ij} = non-linear shear stress

$H(f)$ =Heaviside function

$\delta(f)$ =Dirac delta function

This equation is an extension of Lighthill's acoustic analogy, which was derived to explain the sound generated by a turbulent jet (rather that a moving surface) in a stationary fluid. An important result of the solution of this equation is the coupling of the acoustic pressure generated at the moving surface (left side of equation 1) to noise radiated due to water volume displacement (or thickness noise) in the direction of the observer, to the variations of the surface stress (loading noise) and to the sound radiated by both turbulence and flow distortions such as shock waves, which are associated with the blades (volume noise) [5]. Furthermore, these sources generate two distinct types of acoustic signatures. One is of a periodic nature and occurs at least once every rotation of

7

the propeller and is known as tone or harmonic noise. The other is broadband noise and is of random and non-periodic nature.

On marine propeller blades, the steady and unsteady loads generate the most important noise sources. The sound caused by the rotational motion of the steady loading applies to all propellers but it is a relatively weak source of sound compared to the unsteady loading noise [2]. Unlike loading noise that depends on pressure variations on the surface, thickness noise is a volume displacement source caused by the injection and extraction of fluid by the motion of the blade. Its strength is very directional or dependent on the position of the observer. Thickness noise is not important unless the blade tip Mach number is greater than 0.5 [6]. This means that the tip velocity would have to be at least 750 m/s since sound speed in the ocean is approximately 1500 m/s, this source is not important for marine propellers or water turbines.

2.4 Blade Forces Due To A Sinusoidal Gust

It was established above that the periodic noise of non-cavitaing propellers and water turbines operating at low speeds depends mostly on the unsteady blade loads. These load variations can be divided into unsteady drag and lift and for non-cavitating propellers, operating in a non-uniform flow; the unsteady lift fluctuations are the dominant source of noise. W. R. Sears has given an expression for the lift distribution of rigid airfoil passing through a sinusoidal gust, under the assumptions that: the flow about the airfoil is two dimensional and that every point of the trailing vortices left behind by the airfoil is sufficiently small to be consider to lie upon an x'-axis (figure 1). Sears defined the relative vertical velocity felt on the blade as it passes through the gust as [7].

$$w(x', \tau) = \left[W_o + 2 \sum_{n=-\infty}^{\infty} W_n \cos(n\vartheta) \right] U_e \exp(i\omega\tau) \quad (2)$$

Where

$x' = (C/2) \cos (\vartheta)$

C = the chord of the blade

W_o and W_n = Fourier coefficients

The gust moves past the airfoil with velocity U_e and has a wavelength λ, so $\omega = 2\pi U_e/\lambda$.

The general expression for the lift corresponding was found to be

$$L = \pi\rho C U_e^2 \exp(i\omega\tau) \left[(W_o + W_1) \frac{K_1(\sigma)}{K_o(\sigma) + K_1(\sigma)} + (W_o - W_1) \frac{i\sigma}{2} \right] \quad (3)$$

Where $K_{0,1}$ represent Bessel functions of the second kind with a reduced frequency (σ), defined as $\sigma = C\omega/2U_e$.

2.5 Conclusions

From the review of wind turbine noise it is expected that thumping noises will occur in water turbines due to a supporting structure upstream of the blades. Also, estimates of the broadband noise produced by water turbines will not be possible until base line measurements of their noise levels are made. From the review of marine propellers, there are two types of non-caviting noise caused by rotating blades, thickness and loading noise, however, only loading noise is important in water turbines because of their low tip Mach number.

The prediction of noise from rotating blades can be carried out using Lighthills Acoustic Analogy, which relates loading noise to the unsteady lift on the blades. These unsteady lift variations can be modeled by using thin airfoil theory, which gives an

9

expression for the unsteady lift which is proportional to the upwash velocity encountered by the blade and the well known Sear's function.

The next four chapters of this paper will focus on deriving the expressions for the acoustic field from rotating blades, the unsteady lift and upwash velocity, and the application of these theories to water turbines.

Chapter 3: Ocean Current Turbine Testbed (OCTT)

As a first step to develop the commercial harvesting of the kinetic energy from the

Florida Current, Florida Atlantic University's Southeast National Marine Renewable

Energy Center has designed a small-scale ocean current turbine system. This system

consists of a permanently anchored Mooring an Telemetry Buoy (MTB) with a gravity

anchor, an Ocean Current Turbine Testbed (OCTT) and a twin-hull Observation, Control,

Deployment, Platform (OCDP) (figure 2) [8].

3.1 Ocean Current Turbine Testbed

Two different designs of the OCTT are shown in the top part of figure 3. The

OCTT is a 20 kW open-blade axial-flow horizontal underwater turbine driven by a 3 m

diameter, 3-blade rotor with maximum rotational velocity of 40 RPM. It is intended to

operate for long periods of time in the open ocean near the core of the Florida Current

whose mean current speed near the surface is approximately 1.7 m/s. Two buoyancy

compensation modules are attached to a trussed mast mounted at either the top or bottom

of the main body, providing both buoyancy and stability to the turbine.

3.2 Trussed mast

The focus of this study is to calculate and understand the mechanisms behind the

harmonic loading noise levels produced by the OCCT. The upstream truss mounted on

the turbines plays an important roll in the production of the loading noise because it

induces disturbances on the incoming velocity of the blades, which consequently causes fluctuating forces on the surface of the blades. This structure can also develop vortex shedding, which causes an especial type of unsteady loading noise known as blade vortex interaction (BVI), causing a very loud "thumping" sound [5]. This interaction, however, will not be considered in this study and it is rather left as a topic to be investigated in future works. Figure 4 shows the dimensions of this structure.

3.3 Simplified Turbine

Even though the upstream structure has a triangular shape, the theory to estimate the noise levels will be developed for a single structure shaped like a triangular plate, shown in the bottom part of figure 3. The reason for this is to derive simpler mathematical expressions that can later be adjusted to deal with structures of different characteristics, such as, span, shape and distance from the blades. The estimation of the loading noise levels of the OCTT can be simplified by noting the high aspect ratio the blades, which is defined as the ratio of the span to the blade chord and is 1.5:0.15=10. This high aspect ratio indicates that the flow is nearly independent of the radius, and a two-dimensional strip theory approach is valid [9]. It is also assumed that the blades are thin (thickness to chord ratios of less than 0.1) and can be modeled as flat plates confined to the rotor disk plane (right part of figure 5 and bottom of figure 3). The implementation of this model is based on the assumption that the results for loading noise levels are qualitatively similar for blades whose cross-sections are either thin, flat plates or real hydrofoils [10].

3.3.1 Dimensions

Table 1 shows the dimensions of the model and the rotor needed in the estimation of the noise levels.

RPM	50
Blades Angular Velocity W	$5\pi/3$ rad/s
Free stream Velocity U_∞	1.7 m/s
Radius of the Blade (G)	1.36 m
Radius of the Hub	0.7 m
Blade's Chord	0.15 m
Upstream Structure's Chord	0.30 m
Wynaski Universal Constant Δ_o	1.71
Wynaski Universal Constant W'_o	0.297
Number of blade subsections	B
Total radius of the blade	Γ
Span Step	$\Delta\gamma{=}0.9\Gamma/\,B$
Structure- Blades Distance	1.40 m
Structure's Width	0.86 m

Table 1 Tabulation of the dimensions used in the estimation of the noise levels

3.4 Conclusions

The trussed mast attached to the OCCT is expected to induce changes in the incoming velocity of the blades, which will create a thumping noise similar to that of the downstream wind turbines. The development of the mathematical model of the noise

levels will be based on a simplified version of the existing turbine design, this is done to obtain a simplified, more adjustable mathematical model. The simplified design consists of an upstream structure reduced to a triangular plate and blades considered to be lifting surfaces of the planar type. The results obtained with this description are qualitatively applicable to blades that are not restricted to lie on the rotor's plane.

Chapter 4: Radiated Sound

4.1 Basic Equation

From Chapter Two it was concluded, that the second term of the Ffowcs Wiiliams and Hawkins Equation (Eq 1) describes the dominant source of sound generation by water turbines. On this basis the solution to equation (1) is obtained as [5].

$$p'(\mathbf{x},t) = -\frac{\partial}{\partial x_i} \int_S \left[\frac{P_{ij}n_j}{4\pi r \,|1 - M_r|} \right]_{\tau = \tau*} dS \qquad (4)$$

$\mathbf{x} = [x_1 \ x_2 \ x_3]$ = position of the observer (figure 6)

$r = |\,\mathbf{x} - \mathbf{y}\,| = \sqrt{\left(x_1 - \gamma\cos(\phi)\right)^2 + \left(x_2 - \gamma\sin(\phi)\right)^2 + \left(x_3 - 0\right)^2}$ Distance between acoustic

source and observer

$\mathbf{y} = [\gamma\cos(\phi) \,, \ \gamma\sin(\phi) \,, \ 0]$ position of

the noise source

γ = radius of the point source element

$\phi = \Omega\tau$ time dependent azimuthal

location

Ω = angular speed of the blades

τ = emission time

P_{ij} = surface stress tensor

M_r = Mach number in the radiation

direction.

$\tau* = t - r/c_o$ retarded time or emission

time

c_o = the speed of sound in sea water

S = surface of the blade

Equation 4 gives the dipole term of the Ffowcs Williams and Hawkings equation, which relates the radiated acoustic pressure field generated by the rotor blades to the variations of the compressive stress tensor P_{ij} on the blade surfaces.

4.2 Simplifications and Assumptions

For water turbines, unsteady variations of the drag are small compared to those of the lift [5]. Thus, only the fluctuating forces in the direction perpendicular to the rotor will be important, so in Eq. 4, $n_jP_{ij} = F_i$ can be replaced by F_3 where $i=3$ represents the direction along the rotor axis. Also, since we are assuming strip theory and acoustic compactness (which is reasonable if the ratio of the chord to the acoustic wavelength is less than one) then the chordwise load distributions can be neglected, and the noise sources can be model as a rotating line source as shown in figure 7. So in equation 4, the lift per unit area n_jP_{ij} can be replaced by lift per unit span L, which reduces the surface integral of equation 4 to a line integral along the span of the blade.

Further simplification is obtained by noting that in the acoustic far field, the propagation effects dominate the space derivatives [5], yielding the following approximation

$$\frac{\partial}{\partial x_i} \sim \left(\frac{x_i}{rc_o}\right)\frac{\partial}{\partial t} \quad (5)$$

where t is the observer time. Since the integrand in equation 4 must be evaluated at the emission time $\tau* = t - r/c_o$, where r/c_o is the time the acoustic wave takes to propagate at the speed of sound from the source element to the observer. It is necessary to convert the time differential of the observed field into an expression evaluated at emission time. To do this it is noted that

$t = \tau + r/c_o$ (6)

Differentiating equation 6 with respect to τ gives

$$\frac{\partial t}{\partial \tau} = 1 + \frac{1}{c_o}\frac{\partial r}{\partial \tau} = 1 + \left(\frac{-v_r}{c_o}\right) = 1 - M_r \quad (7)$$

where v_r is the component of the surface velocity in the direction of the observer, and M_r is the Mach number of the source motion in the direction of the observer. The partial derivative with respect to t is then

$$\frac{\partial}{\partial t} = \frac{\partial}{\partial \tau}\frac{\partial \tau}{\partial t} = \left(\frac{1}{1 - M_r}\right)\frac{\partial}{\partial \tau} \quad (8)$$

Substitution of equations 5 and 8 into equation 4 and letting $n_j P_{ij} = L$, yields

$$p'(\mathbf{x}, t) = -\int_\gamma \left[\frac{x_3}{r^2}\frac{1}{4\pi c_o(1 - M_r)^2}\frac{\partial L}{\partial \tau}\right]_{\tau = \tau^*} d\gamma \quad (9)$$

Equation 9 gives the time history of the acoustic field, which is proportional to the unsteady lift variations on the blade. The extra factor of $(1-M_r)^{-1}$ arises as a consequence of the distortion between emitted and observer's time histories, and it can be interpreted as the compression factor between these histories. Physically this means that the rotational motion of a source compresses the observer's time history (with respect to the emitted history) as it moves closer to the observer [5]. This difference between the time histories is caused by a time delay effect produced by distance variations between the noise sources and the observer as the blades rotate. The details of such variations will be the topic of the next section.

4.3 Time Delay Effect

One important thing to notice in the equations above, is the retarded time difference that is specified in equation 9: the integral is evaluated at a fixed observer time t while the lift fluctuations over the surface of the blade vary with emission time τ. This time difference is a result of the time delay between the time a source emits the acoustic pressure and the time it is felt at a point of observation. A depiction of this time delay is shown in figure 7, where the rotor of a water turbine and two rings are shown. The rings are located at about 10 and 90 percent of the blade radius. These rings can be viewed as a series of continuous point sources where the strength on each ring is zero everywhere except at specific locations ϕ along the circular path [6]. For the depiction of figure 6, this specific location is the turbulent wake created by the upstream structure represented by the dashed triangle. Since the turbine is stationary and its blades are rotating at a constant angular velocity (Ω) the source strength will be dependent of the time τ by $\phi = \Omega\tau$. As the blade passes through the wake, each ring creates an acoustic pulse, whose emitted time history can be calculated for a given point in the far field [6]. The problem, however, arises when calculating the observer's time history of the entire blade, because each point source is either a bit closer or farther from the point of observation.

To illustrate this, let r_1 and r_2 represent the distances between the observer and the sources at 10 and 90 percent of the blade, respectively. It can be seen from figure 7, that these distances vary depending on the position of the source with respect to the position of the observer, at a given time. If a ping signal is sent by each of the point sources at the same time, then observer 1 will receive the signal from point source 1 before receiving it from point source 2 and the opposite will happen for observer 2. These retarded arrivals

18

are the cause of the time delays, which creates a difficulty in the calculation of the radiated acoustic time history of the entire blade. This difficulty is dealt with by using linear interpolating methods discussed in the following section.

4.4 Interpolation Method

To evaluate Eq. 9 and account for the time delays, it is necessary to interpolate the results of this equation in the following manner. First, Eq. 9 must be evaluated as if it was a function of constant increments in emission time $\tau = \tau_n = n\Delta\tau$. For the water turbine shown in figure 8, the results of $p'(x, \tau_n)$ can be tabulated for each radius γ_m in the following way

$P'(\tau)$	τ_1	τ_2	τ_3	…	τ_N
γ_1	$P'(\tau)_{11}$	$P'(\tau)_{12}$	$P'(\tau)_{13}$	…	$P'(\tau)_{1N}$
γ_2	$P'(\tau)_{21}$	$P'(\tau)_{22}$	$P'(\tau)_{23}$	…	$P'(\tau)_{2N}$
γ_3	$P'(\tau)_{31}$	$P'(\tau)_{32}$	$P'(\tau)_{33}$	…	$P'(\tau)_{3N}$
.	.	.	.	.	.
.	.	.	.	.	.
.	.	.	.	.	.
$\gamma_{m'}$	$P'(\tau)_{m'1}$	$P'(\tau)_{m'2}$	$P'(\tau)_{m'4}$	…	$P'(\tau)_{m'N}$

Table 2 Tabulated acoustic pressure time history of turbine shown in figure 8

Where each row represents a ring, and each column represents the equally space components of the emitted time history $p'(\tau)$. This can also be represented in Cartesian tensor notation as

$p'(\tau)_{ij}$ (10)

Where

$i = 1,2,3,\ldots,m'$ Number of the ring or blade sections

$\tau_n = n\Delta\tau$. $-N/2 < n < N/2$ Emission time

$T = N(\Delta\tau)$ The period of one revolution

$j = 1$ to N so $n = j - 1 - N/2$

      Equation 10 and table 2 give the acoustic pressure time history of each individual ring, in the far field. To obtain the observer's time history of the entire blade $p'(t')$ it is necessary to sum up the perturbation acoustic pressures at a given point in the far field at the same observer time, from all the rings or sections of the blade. To do this, the results of Eq. 10 will be interpolated to obtain these results at fixed intervals of observer time $t'=m\Delta t$. The linear interpolation method is carried out using the following equation.

$$p'(t'_{m'})_{ij} = \frac{(t'_{ij} - t_{ij})(p'(\tau)_{i(j+1)} - p'(\tau)_{ij})}{(t_{i(j+1)} - t_{ij})} \quad (11)$$

where t_{ij} is the observer time for the jth emission time increment for the ith source ring, and t_m' is the observer time for the m'^{th} observer time increment where $t_{ij} < t_{m'} < t_{i(j+1)}$. The acoustic pressure time history $p'(t')$ is obtained by adding up the signatures for each ring. This operation sums up all the perturbation pressures arriving at the point of observation at particular time t'_m regardless of location of the point source where the perturbations originated.

4.5 Conclusions

      The FW-H equation is reduced to its dipole term in the case of water turbines. This term relates the radiated acoustic pressure caused by the blades to the unsteady

fluctuations on their surfaces. This term can be simplified by realizing that, the unsteady drag fluctuations are negligible, the noise sources can be approximated as line sources, and that propagation effects dominate the space derivatives in the acoustic far field. There is a time delay between the source and observer times, which occurs due to differences in the distances between points on the blade surface and the observer. Linear interpolation methods are required to evaluate the observed signature at a fixed point from the time history of the source on the blade.

Chapter 5: Unsteady Lift Noise

It was shown in the previous chapter, that the radiated sound of a blade is proportional to the unsteady lift fluctuations on its surface. This chapter will give a description and mathematical model of the process by which these fluctuations occur.

5.1 Lift Fluctuations

Unsteady lift fluctuations are induced by small velocity variations w that causes a small change in angle of attack to the blade. In order to get an overview of this process, consider the water turbine design shown in figure 9 (the arrows do not depict any velocity profiles, they are there only to make a distinction between the areas where U and U_∞ interact with the blades), where a lift vector (L) is at the tip of the blade as it goes around the circular path. At the interception with the black triangle, the blade encounters a sudden variation of the inflow velocity caused by the structure upstream of it, inducing an unsteady perturbation lift on the blade (L' in red). This time dependent changing lift causes noise in accordence with Eq. 9

5.2 Lift on a Rigid Airfoil

The high aspect ratio of the OCTT design allows for the use of strip-theory, meaning that the flow past the blade can be described as the flow past each cross-section of the blade. From this, it can be assumed, that the wake past the trailing edge is sufficiently small that every point of the trailing of vortices left behind by the blade may

22

be considered to lie on the x'-axis (figure 1). This assumption allows the use of Von Karman and Sears's general expressions for the lift distribution on an airfoil in non-uniform motion. For the case of the OCTT, it is necessary to use the lift response function for a rigid two-dimensional flat plate passing through a vertical gust in an incompressible flow, which was developed by Sears and is a specialized case of the general expression for lift distribution on an airfoil in non-uniform motion. This expression yields the lift as a function of a non-dimensional variable known as reduced frequency σ, which is defined as π times the ratio of the chord to the wavelength of the gust pattern [7].

5.2.1 Vertical Gust Velocity

Figure 10, shows an idealized model of a vertical gust velocity passing through an airfoil. The vertical gust velocity can be expressed as

$$v(x',\tau) = W\exp(ik_1(x' - U_e\tau) + i\phi)\ (12)$$

In this equation the sinusoidal gust pattern has a maximum magnitude W and a phase shift ϕ. If the gust moves past the foil with velocity U_e and has a wavelength λ then the frequency of the wave ω is defined as

$$\omega = \frac{2\pi U_e}{\lambda} = k_1 U_e \qquad -\frac{C}{2} \le x' \le \frac{C}{2}\ (13)$$

Where C is the chord of the foil and k_1 is the wave number along x'. If $v(x', \tau)$ is positive upwards then Eq. 2 or the vertical velocity (upwash) at any point, measured positive upwards on the foil can be expressed as [7]

$$w(x',\tau) = \text{Re}\left(W\exp\left(ik_1(x' - U_e\tau) + i\phi\right)\right)\ (14)$$

The amplitude of the upwash gust can be defined from the vertical velocity at the point $x'=0$. Combining equation 14 with 13 gives

$$w(0, \tau) = \text{Re}\left(W \exp(-i\omega\tau + i\phi)\right)$$

or

$$w(\tau) = |W| \cos(\omega\tau + \phi) \quad (15)$$

For a more general periodic gust we can define

$$w(\tau) = \sum_{n=1}^{\infty} W_n \cos(n\Omega\tau + \phi_n) = \text{Re}\left(\sum_{n=1}^{\infty} W_n \exp(in\Omega\tau + i\phi_n)\right) \quad (16)$$

and calculate the response to each frequency $n\Omega$

5.2.2 Lift Per Unit Span Equation

From figure 10, the lift per unit span is defined as

$$L(\tau) = \text{Re}\left(L_o \exp(-i\omega\tau + i\vartheta)\right) \quad (17)$$

Where, according to Sears [7]

$$L_o \exp(i\vartheta) = \pi\rho U_e C W S(\sigma)\exp(i\phi) \quad (18)$$

$$\sigma = \pi \frac{C}{\lambda} = \frac{\omega C}{2U_e} \quad (19)$$

$$S(\sigma) = \frac{\left(\dfrac{2i}{\sigma\pi}\right)}{H_1^{(2)}(\sigma) + iH_0^{(2)}(\sigma)} \quad (20)$$

The non-dimensional frequency σ was a parameter used by Sears to analyze the magnitude and phase of the lift. $S(\sigma)$ is the standard two-dimensional Sears function, which relates lift per unit span (L) to the incident amplitude (W) of the upwash and $H_1^{(2)}(\sigma)$ and $H_0^{(2)}(\sigma)$ are cylindrical Hankel functions.

Putting Eq. 18 into 17, the lift per unit span becomes

$$L(\tau) = \mathrm{Re}\left(\pi\rho U_e CW \mid S(\sigma) \mid \exp(-i\omega\tau + i\phi + i\beta(\sigma))\right) \quad (21)$$

where $\beta(\sigma)$ is the phase of the Sears function. Since a periodic gust profile can always be formed by superposition of sinusoidal gusts, as shown above, Eq. 21 can be represented as

$$L(\tau) = \sum_{n=0}^{\infty} \pi\rho U_e CW_n \left| S(\sigma_n) \right| \cos(n\Omega\tau + \beta(\sigma_n) + \phi_n) \quad (22)$$

Where

$$\sigma = \left(\frac{n\Omega C}{2U_e} \right)$$

This is the total lift produced on any rigid airfoil by a vertical gust of any arbitrary profile, which is proportional to the upwash Fourier coefficients and the Sears function.

5.3 Conclusions

The upwash velocity induces unsteady lift fluctuations. The upwash velocity produce these fluctuations by generating a lift perturbation while passing through the wake formed by the upstream structure. The expression for the lift distribution of a rigid airfoil passing through a sinusoidal gust has been given Sears. This expression is proportional to the upwash velocity encountered by the blade and the well-known Sear's function, which depends on a non-dimensional frequency variable. This expression (Eq.21) calls for the Fourier coefficients of the upwash velocity, which will be calculated by taking advantage of the periodicity of the blade motion. The details of these calculations and the derivation of the upwash velocity from the velocity deficits induced by the upstream structure will be the topics of Chapter Six.

Chapter 6: Velocity Deficits and Upwash Velocity

From Chapter Five, the expression of the unsteady lift based on Sear's theory

depends on a vertical velocity relative to the blade surface known as the upwash velocity.

The upwash velocity causes changes in the angle of attack, and is generated by incoming

velocity disturbances originated at the structure upstream of the blades. This chapter will

present, first, the modeling of the velocity profile of these velocity disturbances by using

I. Wygnanski, F. Champagne and B. Marasli's theory [11]. Then, a description of the

mechanisms responsible for the changes in angle of attack due to the velocity

disturbances will follow. Finally, the expression of the velocity profile downstream of a

structure and the description of the interacting velocities affecting the blade will be used

to derive an expression for the upwash velocity. Sear's expression of the lift (Eq. 22)

calls for the Fourier coefficients of the upwash velocity, which are calculated by taking

advantage of the periodicity of the blade motion.

6.1 Velocity Deficit Profile

The velocity deficit profile originates at the upstream structure and is modeled by

using the results of Wygnanski, Champagne and Marasli's for two-dimensional,

turbulent, small deficit wakes crated by wake generators of different shapes. From this

study it was shown that, at a distance far enough, downstream of the wake generator

(approximately 100 to 2000 wake momentum thicknesses), an asymptotic self-preserving

state is achieved. Furthermore, this self-preserving state can be described by a single

velocity scale u_o and a length scale L_o (Figure 11). The self-similar mean velocity field $U(y)$ used in solving the governing equations was obtained experimentally and expressed by the exponential distribution.

$$U = U_e - u_o \exp(-0.693\eta^2) = U_\infty - U_t \quad (23)$$

Where u_o is the maximum velocity deficit, U_t is the velocity perturbation, the free stream velocity is U_∞ as shown in figure 11, and

$$\eta = \frac{y}{L_o} \quad (24)$$

$$L_o = \Delta_o \sqrt{\theta(x - x_o)} = \text{Length scale} \quad (25)$$

$$u_o = U_\infty W_o' \sqrt{\frac{\theta}{(x - x_o)}} = \text{Velocity scale} \quad (26)$$

$$\theta = \frac{C_d d}{2} = \text{Momentum thickness of the wake} \quad (27)$$

$\Delta_o = 1.71$ and $W'_o = 0.297$ are universal constants determined experimentally.

$x - x_o$ = structure-blades distance, where x_o is a virtual origin which varies from structure to structure

C_d = Coefficient of drag

d = Width of the wake generator

Equation 23 is a description of the velocity profile approaching the blades after passing by the upstream structure. This reduced velocity profile or wake causes changes in the incoming velocity of the blades as it passes through it; it is during the crossing of this profile that the upwash velocity perturbations arise. The description of this occurrence will be the topic of the next section.

6.2 Velocities (U_∞, U, V, U_e and w) and Angle of Attack (α)

In order to understand how the upwash velocity w arises during the operation of the OCTT, it is necessary to understand the interaction of the different velocity vectors acting on the blades as it passes through the reduced velocity profile. If the turbine is operating in a uniform flow with free stream velocity U_∞, angular velocity Ω and angle of attack α then the incoming local velocity U_e in a hydrofoil section is dipicted in figure 12. Figure 12 is a representation of U_e outside the wake. Figure 13, on the other hand, shows what happens when the blade passes through the wake. Each section experiences a reduction of its incoming velocity U_e, this is because the velocity parallel to the rotor U_∞ is reduced by a velocity perturbation U_t (figure 13). This creates a new incoming velocity U'_e (figure 13), which in turn produces a change in the angle of attack. Slow changes in angle of attack are unimportant, but when the blade encounters rapid or sudden variations of this angle, the unsteady lift source becomes very efficient 5]. This is because as the blade passes through the velocity profile of the wake it experiences a continuous change of the incoming velocity U_e, increasing the magnitude of the derivative term in Eq. 9.

6.3 Upwash as a Function of Time

Figure 13 shows the vector geometry of the upwash velocity with the rest of the velocity vectors interacting with the blade. From the vector diagram of figure 14, it can be seen that

$$\sin(\varphi) = \frac{\Omega \gamma}{U_e} = \frac{w}{U_t} \quad (28)$$

Where γ is the radius of a given section of the blade and the incoming velocity U_e is defined as

$$U_e = \sqrt{(U_\infty)^2 + (\Omega\gamma)^2} \quad (29)$$

Rearranging and solving for w

$$w = U_t \frac{\Omega\gamma}{U_e} \quad (30)$$

Putting equations 28 and 29 into 30, w is defined as

$$w = u_o \exp(-0.693\eta^2)\frac{\Omega\gamma}{U_e} \quad (31)$$

Also, it can be seen in figure 6 that for small angles (ψ) Eq. 23 becomes

$$\eta = \frac{y}{L_o} = \frac{\gamma\psi}{L_o} = \frac{\gamma\Omega\tau}{L_o} \quad (32)$$

Finally combining equations 31 and 32 yields the upwash vertical velocity as a function of time.

$$w(\tau) = u_o\left(\frac{\Omega\gamma}{U_e}\right)\exp\left(-0.693\left(\frac{\Omega\gamma\tau}{L_o}\right)^2\right) \quad (33)$$

6.3.1 Fourier series expansion of the upwash (w)

With an expression for the upwash velocity on the blades obtained as function of time, we can now calculate the Fourier coefficients called for by Eq. 22. Noting that w is a periodic function, since it occurs once in every rotation, and letting constants C_o and C_1 be defined as

$$C_o = u_o\left(\frac{\Omega\gamma}{\sqrt{U_e^2 + (\Omega\gamma)^2}}\right) \quad (34)$$

$$C_1 = 0.693\left(\frac{\Omega\gamma}{L_o}\right)^2 \quad (35)$$

Equation 33 can be expressed in the following form.

$$w(\tau) = C_o \exp(-C_1\tau^2) \quad -T/2 \le \tau T/2 \ (36)$$

a plot of Eq. 36 is shown in left part of figure 15. The period is defined as

$$T = \frac{2\pi}{\Omega} \ (37)$$

Since $w(\tau)$ is symmetrical about the ordinate its Fourier series can be represented as

$$w(\tau) = \frac{W_o}{2} + \sum_{n=-\infty}^{\infty} W_n \cos(n\Omega\tau) \ (38)$$

which implies that ϕ_n is zero in Eq. 22, and where

$$W_n = \frac{1}{(T/2)} \int_0^T w(\tau)\cos(n\Omega\tau)d\tau = 2\,\mathrm{Re}\left(\frac{1}{T}\int_0^T w(\tau)\exp(-in\Omega\tau)d\tau\right) \ (39)$$

One thing to notice here is that the interval of Eq. 36 is defined as

$-T/2 \le \tau \le T/2$ whereas the integral of Eq. 39 calls for the integration on the interval

$0 \le \tau \le T$. To adjust for this difference, Eq. 36 is shifted in the following way

$$w(\tau) = C_o\left(\exp(-C_1\tau^2) + \exp(-C_1(T-\tau)^2)\right) \quad 0 \le \tau \le T \ (40)$$

Plot of Eq. 40 is shown in the right part of figure 15. Also, integration of Eq. 39 can be

approximated as.

$$W_n \approx 2\,\mathrm{Re}\left(\frac{1}{T}\sum_{m=0}^{M-1} w(m\Delta\tau)\exp(-in\Omega m\Delta\tau)\Delta\tau\right) \quad n < \frac{M}{2} \ (41)$$

To calculate Eq. 41 using the Matlab routine (ifft), $\Delta\tau$ and Ω will be defined in the

following manner

$$M\Delta\tau = T \ (42)$$

$$\Omega = \frac{2\pi}{M\Delta\tau} \ (43)$$

30

Substituting equations (42) and (43) into (41) yields:

$$W_n \approx 2\operatorname{Re}\left(\frac{1}{M}\sum_{m=0}^{M-1}w(m\Delta\tau)\exp\left(-\frac{2i\pi mn}{M}\right)\right) = 2\operatorname{Re}\left(ifft(w(m\Delta\tau))\right) \quad (44)$$

In this case, Eq. 44 represents the Fourier coefficients of the vertical velocity on a rigid flat plate passing through a sinusoidal gust. Eq. 22 relates these coefficients to the lift distribution on the blades.

6.4 Conclusions

The upstream structure reduces the free steam velocity; the profile of this reduced velocity can be model using two scaled characteristics whose value depends on the shape of the structure. The reduction of the free stream velocity causes changes in the incoming velocity of the blades, which gives rise to the upwash velocity. The upwash velocity creates the changes in angle of attack responsible for the lift fluctuations related to the radiated acoustic pressure.

Chapter 7: Results and Discussions

Chapter Four described the FW-H equation, which can be used to relate the

radiated acoustic pressure from a water turbine to the lift fluctuations on the blades.

Chapter Five discussed the expression for the Sears' unsteady lift distribution of a rigid

airfoil passing through a sinusoidal upwash gust, and then Chapter Six gave the equation

of the upwash velocity and its Fourier coefficients for a typical turbine inflow. In this

chapter, we will bring all these concepts together, and apply them to the simplified

turbine described in section 3.3.

7.1 Combined Results

The results obtained in chapters 4, 5 and 6 are related by the FW-H equation given

by Eq. 9. The first step, we will take to combine these results is to represent the time

derivative of the lift per unit span using Eq. 22 and Eq. 38, in the following way

$$\frac{\partial L}{\partial \tau} = \mathrm{Re}\left(\sum_{n=1}^{\infty} \pi \rho U_e C W_n S(\sigma_n)(-in\Omega)\exp(-in\Omega\tau)\right) \quad (45)$$

Putting Eq. 45 into Eq. 9, we obtain

$$p'(\mathbf{x},t) = \int_{\gamma}\left[\frac{x_3}{r^2}\frac{\rho U_e C}{4c_o(1-M_r)^2}\mathrm{Re}\left(\sum_{n=1}^{\infty} W_n S(\sigma_n)(in\Omega)\exp(-in\Omega\tau)\right)\right]_{\tau=\tau^*} d\gamma \quad (46)$$

where

$$W_n = 2\mathrm{Re}\left(\frac{1}{T}\int_0^T u_o\left(\frac{\Omega\gamma}{U_e}\right)\exp\left(-0.693\left(\frac{\Omega\gamma\tau}{L_o}\right)^2\right)\exp(-in\Omega\tau)d\tau\right) \quad (47)$$

Eq. 47 can be evaluated using the Matlab routine (ifft) shown in Eq. 44. The FW-H equation (Eq. 46) will be used to estimate the unsteady noise levels produced by the simplified water turbine described in Sec 3.3

7.2 Results Applied to a Simplified Turbine

The simplified turbine described in Sec 3.3 has a triangular plate, divided in to B subsections, replacing the upstream structure of the original design, as shown in figure 16. To calculate the noise levels of this design, first, we will find the Fourier coefficients of the upwash velocity using the methods of Sec. 6.3.1. Next, we will determine the position of the observer and use it to find the expressions for r, x_3 and M_r. Next; we will find an expression for the lift's time derivative (Eq. 45) and put it together with the rest of the results into the FW-H equation (Eq. 46). Then the time history of the acoustic field will be used to calculate the frequency spectrum from the signal. Finally, the power spectrum is presented on a decibel scale and corrected for the transmission losses to obtain the effective source levels.

7.2.1 Upwash Velocity (Ideal Turbine)

To obtain the expression for the upwash velocity (Eq. 33) of the simplified turbine, it is necessary to find the coefficient of drag needed in Eq. 27, describing the momentum thickness θ. The coefficient of drag for a plate of width d (as shown in Fig. 16) is $C_d = 2$ [7]. The rest of the parameters needed to complete Eq. 33 for this particular turbine design are tabulated in Table 3.

RPM	50

Blades Angular Velocity Ω	$5\pi/3$ rad/s
Period T	1.2 s
Free stream Velocity U_∞	1.7 m/s
Structure-Blades Distance $(x\text{-}x_o)$	1.43 m
Radius of the Blade (Γ)	1.43 m
Radius of the Hub	0.7 m
Blade's Chord C	0.15 m
Wynaski Universal Constant Δ_o	1.71
Wynaski Universal Constant W'_o	0.297
Number of subsections B	10
Span Step	$\Delta\gamma=0.9\Gamma/B$
Max Structure's Width coinciding with blades d_{max}	0.5 m
Coefficient of drag C_d	2
Observer's position (r_o, θ_o, ϕ_o)	(100 m, 45°, 45°)
Blade's Chord C'	0.05 m

Table 3 Values used in the expression for the upwash velocity of the idealized turbine

Using the values of table 3 and following the procedures presented in section 6.3.1, where C_o and C_1 are defined by Eq. 34-35. The time-shifted equation of the upwash velocity is

$$w(\tau) = C_o(\gamma)\left(-\exp(C_1(\gamma)\tau^2) + \exp(-C_1(\gamma)(T-\tau)^2)\right) \quad 0 \le \tau \le T \quad (48)$$

Notice that C_o and C_1 are functions of γ. Equation 48 gives the upwash velocity felt at a given subsection (figure 17) of the blade, where u_o and L_o depend on the structure's width d. From figure 17, it can be seen that d and γ are related by.

$$d = \frac{\gamma}{2.86} \qquad (49)$$

The Fourier coefficients of $w(\tau)$ are calculated straightforwardly by using Eq. 44

$$W_n \approx 2\operatorname{Re}\left[ifft\left(w(m\Delta\tau)\right)\right] \quad (50)$$

7.2.2 Position of the Observer

If we place the observer in front of the hub at spherical coordinates $(r_o, \theta_o, \phi_o) = (100 \text{ m}, 45°, 45°)$, where the azimuth angle ϕ_o is measured relative to the X_1 axis (figure 16), the elevation angle θ_o is measured relative to the X_3 axis and the distance measured from the hub is denoted by r_o. Then from Sec. 4.1 and Eq. 7, we can define the following terms, found in Eq. 46

$X = [x_1, x_2, x_3]$

$$r^2 = \left(x_1 - \gamma\cos(\phi)\right)^2 + \left(x_2 - \gamma\sin(\phi)\right)^2 + \left(x_3\right)^2 \quad (51)$$

$$M_r = \frac{1}{c_o}\frac{\partial r}{\partial \tau} = \frac{\Omega\gamma}{rc_o}\left(x_1\sin(\Omega\gamma) - x_2\cos(\Omega\gamma)\right) \quad (52)$$

7.2.3 Unsteady Lift (Simplified Turbine)

Next, we find an expression of the time derivative of the lift per unit span of the simplified turbine. By replacing the infinite upper bound of summation for a power-of-two-length, $N=2^9$, we can approximate Eq. 45 as the sum over 512 terms. Also, it can be seen that, the lift per unit span can be obtained by dividing Eq. 45 by a factor of $(-in\Omega)$.

35

By summing the contribution from each subsection of the blade, say, from 10% of the

blade radius to its tip, as shown in figure 17 (not to scale), we can obtain the total lift. If

the blade is broken down into B subsections coinciding with the subsections of the

structure as in Fig. 17, adding each subsection's lift gives

$$L_{total} = \sum_{b=1}^{B} \left(\text{Re} \sum_{n=1}^{512} \pi \rho U_e(b\Delta\gamma) W_n(b\Delta\gamma) S(\sigma_n(b\Delta\gamma)) \exp(-in\Omega\tau) \right) \Delta\gamma \quad (53)$$

Figure 18 shows a plot of the total unsteady lift coefficient (for one blade) against the

emission time τ divide by the period T, for the simplified Turbine

7.2.4 Acoustic Pressure Time History (Ideal Turbine)

By putting the expressions in (51-52) and Eq. 53 into Eq. 46, we can approximate the far

sound signal as

$$p'(\mathbf{x},t) = \sum_{b=1}^{B} \left[\left(\frac{x_3 \rho c}{4c_o} \right) \left(\frac{U_e(b\Delta\gamma)}{r^2(b\Delta\gamma)} \right) \left(\frac{1}{(1-M_r)^2(b\Delta\gamma)} \right) \left(\frac{\partial L(b\Delta\gamma)}{\partial \tau} \right) \right]_{\tau=\tau*} (\Delta\tau) \quad (54)$$

Where

$$\Delta\gamma = \frac{0.9\Gamma}{B} \quad (55)$$

and Γ is the turbine radius. To follow the methods of Sec. 4.4, we evaluate the terms

inside the brackets of Eq. 54 in emission time (rather than observers' time), to obtain the

acoustic time history in the form of Eq. 10 or $p'(\tau)_{ij}$ (see Table 1). These results are then

interpolated by implementing Eq. 11, using the Matlab routine (interp1). Once the

interpolation is done, the acoustic pressure time history $p'(t)$ (dropping the prime of t in

Eq. 11) is obtained by adding up all the pressures occurring at the same times and then

multiplying them by $\Delta\gamma$, in accordance with Eq. 54. This operation yields all the perturbation pressures arriving at the point of observation at particular time t_m regardless of location of the point source where the perturbations originated. Time history $p'(t)$ is shown in figure 19.

7.3 Power Levels

The average power in the acoustic radiated signal $p'(t)$ is either given by the time average of the squared magnitude of the signal, or by the sum of the squared magnitudes of its Fourier coefficients. This relationship is known as Parseval's theorem. The frequency plot of the squared magnitudes of these coefficients gives the power spectral density of the signal or the power distribution over frequency range with dimensions of power divided by Herz. The average power (P') can be express as [12]

$$\mathbf{P}' = \frac{1}{T}\int_T |p'(t)|^2 \, dt = 2\sum_{n=0}^{\infty} |p_n|^2 \quad (55)$$

where p_n is

$$p_n = \frac{1}{T}\int_0^T p'(t)\exp(-in\Omega t)dt \qquad (56)$$

The power contained in any limited frequency range is obtained by summation of the power spectral density over that range, and will be equal to the sum of the Fourier coefficients $|p_n|^2$ whose frequency lies in the range of interest.

7.3.1 Power Levels (Simplified Turbine)

The first thing to notice here is that the Fourier coefficients of the periodic function $p'(t)$, found in Sec 7.2.4, can be calculated using the Matlab routine (ifft). The problem, however, is that this function is defined for the time interval $-T/2<t<T/2$, while

37

Eq. 56 above is defined for the interval $0<t<T$. So, before applying the ifft Matlab routine, it will be necessary to make the following manipulations. First, we introduce a new variable defined as $t''=t + T$ for $T/2<t''<T$, and define $p_{n'}$ as the Fourier coefficients of $p'(t)$. With this new variable we can express Eq. 56 in the following way

$$p_n = \frac{1}{T}\int_0^{T/2} p'(t)\exp(-in\Omega t)dt + \frac{1}{T}\int_{T/2}^T p'(t''-T)\exp(-in\Omega(t''-T))dt'' \qquad (57)$$

since

$$\exp(-in\Omega T) = \exp\left(-in\Omega\frac{2\pi}{\Omega}\right) = 1$$

Eq. 57 becomes

$$p_n = \frac{1}{T}\int_0^{T/2} p'(t)\exp(-in\Omega t)dt + \frac{1}{T}\int_{T/2}^T p'(t''-T)\exp(-in\Omega t'')dt'' \qquad (58)$$

where

$$p'(t) = p'(t''-T) \text{ For } -T/2 < t < 0$$

Bearing this in mind, and approximating Eq. 56 in the same manner as Eq. 41, we obtain

$$p_n = \frac{1}{T}\sum_{m=1}^M p'(m\Delta t)\exp(-in\Omega m\Delta t)\Delta t = \frac{1}{N}\sum_{m=1}^M p'(m\Delta t)\exp(-2\pi inm/M) \qquad (59)$$

It can be seen from Eq. 58 and 59 that

$$p_n = [p_{n'}, p_{n'-N}] \quad (60)$$

where, $p_{n'}$ are the values corresponding to $1<m<M/2$, $p_{n'-M}$ corresponding to $M/2<m<M$ and $T=M\Delta t$. Thus Eq. 60 can be obtained by applying the ifft(ffshift($p'(t)$))) Matlab routine.

7.4 Source Level Power Spectrum

In underwater acoustic systems it is customary to characterize the strength of a source in terms of the intensity produced at a fixed reference range from the source. When converted to a decibel level, this source is called the source level (*SL*). The intensity level (*SE*) due to an excess perturbation or radiated pressure at any range *r* from a compact source in a homogeneous lossless medium is obtain from the source level as follows [12]

$$SE = SL - 20\log_{10}\left(\frac{r}{r_{ref}}\right) \quad (61)$$

Where the range-dependent term is called the transmission loss. *SE* is actually the sound pressure level (*SPL*) of the radiated pressure or excess pressure *p'(t)*, *SE* is defined as

$$SE = SPL = 10\log_{10}\left(\frac{p'_{rms}}{p_{ref}}\right)^2 \quad (62)$$

where $p_{ref} = 1\mu Pa$. From equation 55 it can be seen that

$$\mathbf{P'} = \frac{1}{T}\int_T |p'(t)|^2 \, dt = (p'_{rms})^2 = 2\sum_{n=0}^{\infty} |p_n|^2 \quad (63)$$

Combining equations 61 and 62 and after performing some algebraic manipulations the source level power spectrum is defined as

$$SL = 20\log_{10}\left(\frac{\sqrt{2}\,|p_n|}{p_{ref}}\right) + 20\log_{10}\left(\frac{r}{r_{ref}}\right) \quad (64)$$

Figure 20 shows the noise spectrum levels for the idealized turbine

7.5 Discussions

Figure 18 shows the total perturbation lift coefficient of each of the blades of the simplified turbine. This perturbation lift is caused by the changes in angle of attack while the blades pass by the wake formed by the upstream structure (it is the magnitude of the red arrow in Fig 9). Figure 19 shows the acoustic pressure radiated by the blades as they experience changes in lift (in accordance with Eq. 56), whose magnitude depends on the lift perturbations described above. The acoustic pressure is measured at a point with spherical coordinates (100 m, 45º, 45º) where the origin (0,0,0) is located at the center of the turbine's hub. The maximum pressure is 0.0125 Pa and the minimum is -0.0163 Pa, resulting in a pressure difference of 0.0288 Pa. This pressure difference determines the perceived volume, which is better represented by the noise spectrum shown in figure 20. Figure 21 was taken from [12] and shows the noise levels of long distance shipping in the ocean. Comparing figures 20 and 21, it can be seen that the noise source levels are well above the ambient noise levels in the ocean at very low frequencies (<20Hz), which indicates that the acoustic pulses generated during the operation of the hydrokinetic turbines will certainly be heard in the vicinity of the turbine. However at high frequencies, the noise levels are well below the ambient noise levels in the ocean. Also, noise source levels decrease with range as 6 dB per doubling of distance and so the turbine noise level will not be as significant source of sound at larger distances from the turbine. However the very low frequency nature of the sound may make it particularly audible, and of more significance than similar sound levels at higher frequencies.

7.6 Conclusions

The results found in chapters 4,5 and 6 are combined to derive the FW-H equation, which yields the time history of the acoustic perturbation pressure generated by unsteady lift fluctuations. The average power of this signal is found by summing up the squared magnitudes of its Fourier coefficients. The power spectrum is presented on a decibel scale and corrected for the transmission losses to obtain the effective source levels. The results found in this chapter were obtained for a specific width, coefficient of drag and position of the observer. The source levels of these results were compared to those of the ocean and it was concluded the acoustic pulsations generated under this conditions would be heard in the ocean but only at low frequencies. This conclusion, open questions as to how these results would vary if the characteristics of this problem were to be change. In the next chapter it will be shown how would the results vary, if the shape, width (d) and the position of the observer were changed.

Chapter 8: Alternative Designs

In the preceding chapter, the noise levels of a simplified version of the original turbine design were presented. In this chapter, the simplified design will be modified, by varying its span d, coefficient of drag C_d, structure-blade distance (x-x_o) and location of the observer's position. A plot of the maximum acoustic pressure against the varying characteristic will provide an insight into what improvements can be made to existing turbine designs to reduce the noise levels.

8.1 Acoustic Pressure vs. width (d)

The width d of the simplified model depended on the span of the structure (Fig. 17), and was related to the radius of the blades by Eq. 49. In this section we will make the width uniform as shown in figure. 22, and vary it's width d from 2.54E-2 to 0.5 meters at increments of 2.54E-2 meters (1to 20 inches at increments of 1 inch). Figure 23 shows the plot of the maximum acoustic pressure at each width increment, for an observer positioned at (100 m, 45°, 45°) and parameters tabulated on table 3. It can be seen in the figure that the maximum acoustic pressure increases with increasing width of the support structure. Figure 24, shows the noise spectra for three different widths (0.0254 m, 0.254 m and 0.4826 m). It can be seen in this picture that for small values of d the noise levels are reduced at low frequencies and become more important at larger frequencies (> 15 Hz). When compared to the ambient noise levels shown in Figure 21 [12], it is seen that the thinnest structure, d =0.0254 m, has frequency content in the 20-30Hz frequency

range which is clearly above the ambient noise levels at the same frequency. The significance of this result will depend on the hearing characteristics of the marine life of concern, which may be more sensitive at 30Hz than at 10 Hz. Hence, although the thinner structure generates lower peak pressures, the high frequency content of the sound is much greater and this may have a greater impact on marine life.

Also, it is important to realize that vortex shedding may develop in a structure like that of Fig. 22, for Reynolds numbers in the range of 60 to 10,000 and sometimes even higher. If vortex shedding is generated, it will cause an especial case of unsteady loading noise known as blade vortex interaction (BVI), which produces a local, very rapid, change in angle of attack and a sudden change in the blade load, causing a very loud, dominant "thumping" sound [5]. This interaction, however, will not be considered in this study and it is rather left as a topic to be investigated in future works.

8.2 Acoustic Pressure vs. Coefficient of Drag (C_d)

Different drag coefficients imply different cross-sectional shapes of the mast (Fig. 25). The coefficient of drag was made to vary from $C_d = 0.1$ for a streamline body [7] to $C_d = 2$ for a flat plate, at increments of 0.1. Figure 26, shows the plot of maximum acoustic pressure vs. C_d, for an observer positioned at (100 m, 45°, 45°) and parameters tabulated on table 3, except for the width, which in this case was taken to be $d = 0.0254$ m. The acoustic pressure increases with increasing C_d. so in order to reduce the maximum noise levels, the structure's cross section should be as streamlined as possible. Figure 27, shows the noise spectra for three cross sectional shapes of different drag coefficients (C_d = 0.1, 1, 2). It can be seen in this picture that for streamlined cross sections, the noise

levels get significantly reduced, however, they become more important at higher

frequencies (> 45 Hz), but are always below the background noise levels.

8.3 Acoustic Pressure vs. Structure-blade Distance (x-x_o)

The distance between structure and the blades (x-x_o) shown in figure 25 was varied

from 1 to 2 meters at increments of 0.1 meters. Figure 26 shows the plot of maximum

pressure vs. (x-x_o), for an observer positioned at (100 m, 45º, 45º) and parameters

tabulated on table 3, except for the width and coefficient of drag, which in this case were

taken to be $d = 0.0254$ m and $C_d = 0.1$. It can be seen in the figure that increasing the

distance between the structure and the blades reduces the maximum acoustic pressure.

Figure 29, shows the noise spectra for three different structure-blade distances ((x-x_o) =

0.1 m, 1 m, 2 m). It can be seen that for larger distances the noise levels are reduced (this

reduction is less significant than that caused by C_d and d). However, this noise levels

reduction becomes more and more significant at higher frequencies (> 30 Hz)

8.4 Acoustic Pressure vs. Angle to Rotor Axis (θ_o)

The acoustic pressure as a function of the angle of the observer to the rotor axis is

plotted from 0º to 90º in Figure 30 (for the parameters used in the last section). The

acoustic pressure decreases with increasing elevation angle and the important thing to

notice is the directionality of the sound; the maximum amount of energy of the signal is

detected along the rotor axis perpendicular to the rotor's disk whereas the weakest signal

is radiated in the direction parallel to the disk plane. This can be seen in figure 31, where

the noise levels along the disk plane ($\theta_o = 90º$) are considerably reduced in comparison to

those in the direction along the rotor axis ($\theta_o = 0°$). This indicates that the water turbine has the characteristics of an axial dipole.

8.5 Discussions

The upstream structure of an ideal water turbine designed to reduce the noise levels generated by unsteady lift fluctuations on the blade due to blade incoming velocity disturbances will need to have the following characteristics.

1) The width should be kept as narrow as possible

2) The cross section of the structure should be streamlined

3) The structure-blade distance should be as large as possible

Due to the directionality of the sound, the noise levels would be greater when the observer is located on the rotor axis

One important thing to remember here is that changing some of these characteristics will reduce appreciably the noise levels at low frequencies, while moderately increasing the noise levels at higher frequencies.

Chapter 9: Conclusions

This investigation began with the motivations to; first, provide a description of the physical mechanisms behind the generation of water turbine noise, and second, to develop a mathematical model that will provide estimates of the noise levels. These noise level predictions can be used to assess the environmental impact of water turbine noise and to provide an insight into what improvements can be made to existing turbine designs to reduce the noise levels.

From studies on wind turbine and marine propellers noise, it is expected that water turbines will generate two types of acoustic signatures, harmonic noise and broadband noise. The harmonic noise is expected to dominate and so it became the focus of this study. According to the FW-H equation, the harmonic noise generated by water turbines can be predicted by its dipole term, which depends on the loading fluctuations on the blade. These loading fluctuations can be decomposed into a drag and lift fluctuation components, which can occur either in a steady or unsteady manner. Both steady and unsteady fluctuations are expected to occur in water turbines, however, it is expected that the unsteady lift fluctuations will be the dominant source of noise for water turbines. The lift fluctuations are created by changes in the angle of attack caused by velocity disturbances originated at the structure upstream of the blades.

This mathematical model was developed under the assumption that the blades were of the planar type or restricted to lie on the rotor disk plane, which allowed for the

46

use of thin airfoil theory. This assumption is justified by the fact that the results obtained

with this description are qualitatively applicable to blades of arbitrary thickness.

The mathematical model provided in this paper relies on the FW-H equation predicting

the time history of the acoustic pressure radiated during the passage of the blades through

a wake formed in the upstream structure attached to the turbine. The acoustic pressure

was first calculated for an observer located a point within the vicinity of a turbine (100 m,

45°, 45°) with a simplified upstream structure. This simplification was made to obtain a

preliminary estimation of the noise levels produced by the original turbine design. These

noise levels were compared to the ambient noise levels in the ocean and it was found that;

at very low frequencies (< 20Hz) the simplified turbine noise levels surpassed the

ambient noise levels. This indicates that the acoustic pulses generated during the

operation of a water turbine with these characteristics will certainly be heard in the

vicinity of the turbine. However at high frequencies, the noise levels were found to be

below the ambient noise levels in the ocean. Also, noise source levels decrease with

range as 6 dB per doubling of distance and so the turbine noise level will not be as

significant source of sound at larger distances from the turbine. However the very low

frequency nature of the sound may make it particularly audible, and of more significance

than similar sound levels at higher frequencies. This conclusion opened questions as to

how these results would vary if characteristics of the structure upstream of the rotor were

changed. The width of the structure was varied from 2.54E-2 to 0.5 meters at increments

of 2.54E-2 meters (1to 20 inches at increments of 1 inch), for an observer positioned at

(100 m, 45°, 45°). The results obtained from the width variation showed that; the

maximum acoustic pressure increases with increasing width of the support structure, for

small values of the width the noise levels are reduced at low frequencies and become more important at larger frequencies (> 15 Hz) and that for a thinnest structure, of width 0.0254 m. The frequency content in the range 20-30Hz is clearly above the ambient noise levels at the same frequency. The significance of this result will depend on the hearing characteristics of the marine life of concern, which may be more sensitive at 30Hz than at 15 Hz. Hence, although the thinner structure generates lower peak pressures, the high frequency content of the sound is much greater and this may have a greater impact on marine life.

Different drag coefficients imply different cross-sectional shapes of the structure. The coefficient of drag was varied from $C_d = 0.1$ for a streamline body [7] to $C_d = 2$ for a flat plate, at increments of 0.1, for an observer positioned at (100 m, 45°, 45°). The results obtained from the variation of C_d showed that the acoustic pressure increases with increasing C_d. so in order to reduce the maximum noise levels, the structure's cross section should be as streamlined as possible. For streamlined cross sections, the noise levels get significantly reduced, however, they become more important at higher frequencies (> 65 Hz), but are always below the background noise levels. The structure-rotor distance (x-x_o) was varied from 1 to 2 meters at increments of 0.1 meters, for an observer positioned at (100 m, 45°, 45°). The results obtained from the variation of (x-x_o) showed that increasing the distance between the structure and the blades reduces the maximum acoustic pressure, but this reduction is less significant than that caused by C_d and d. However, the noise levels reduction becomes more and more significant at higher frequencies (> 30 Hz).

Varying the angle to rotor axis (elevation angle θ_o) from 0° to 90° changed the position of the observer. The results of the variation of θ_o showed that; the acoustic pressure decreases with increasing elevation angle, which dictates the directionality of the sound. The maximum amount of energy of the signal is detected along the rotor axis perpendicular to the rotor's disk whereas the weakest signal is radiated in the direction parallel to the disk plane, which indicates that the water turbine has the characteristics of an axial dipole as expected from the FW-H equation.

Thus, the upstream structure of an ideal water turbine designed to reduce the noise levels generated by unsteady lift fluctuations on the blade due to blade incoming velocity disturbances will need to have the following characteristics.

 1) The width should be kept as narrow as possible

2) The cross section of the structure should be streamlined

3) The structure-blade distance should be as large as possible

Due to the directionality of the sound, the noise levels would be greater when the observer is located on the rotor axis

One important thing to bear in mind, while deciding on the design-modifications that are needed to reduce the noise levels of existing turbine designs, is the hearing characteristics of the marine life of concern whose sensitive may vary across the frequency domain, because changing some of the characteristics listed above will only appreciably reduce the noise levels at low frequencies, while moderately increasing the noise levels at higher frequencies.
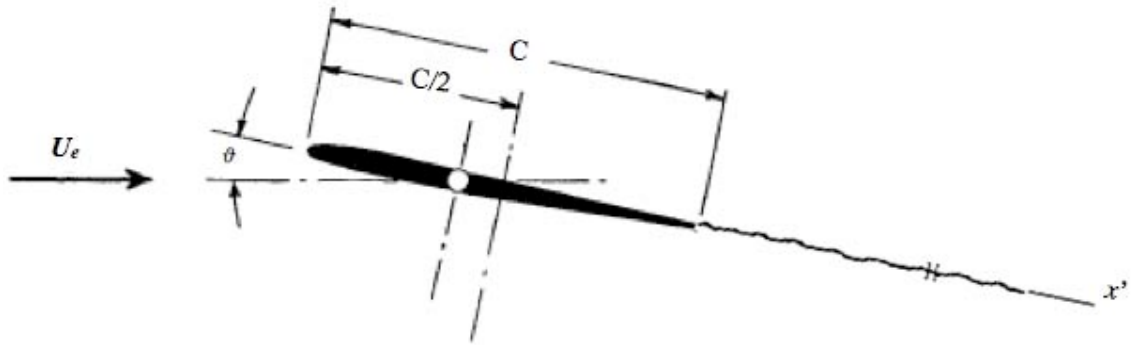
Figure 1 Diagram showing the notation employed
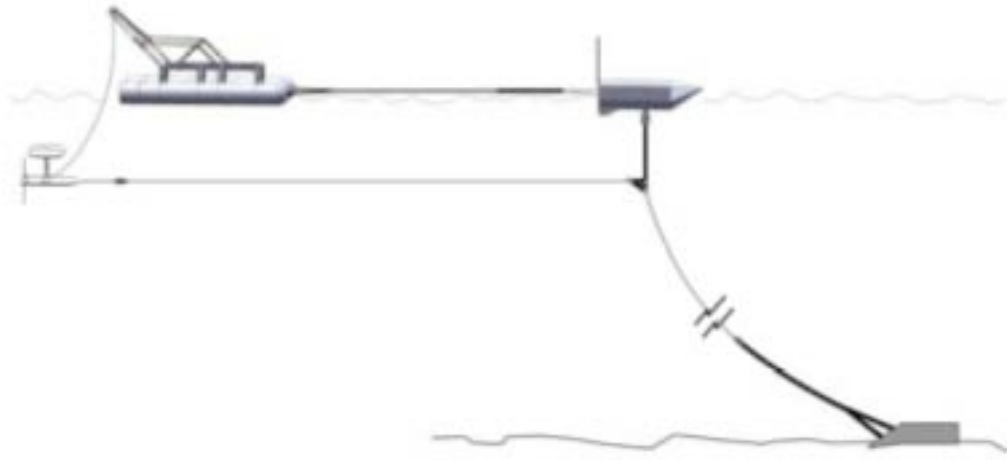
Figure 2 Ocean Current Test Bed
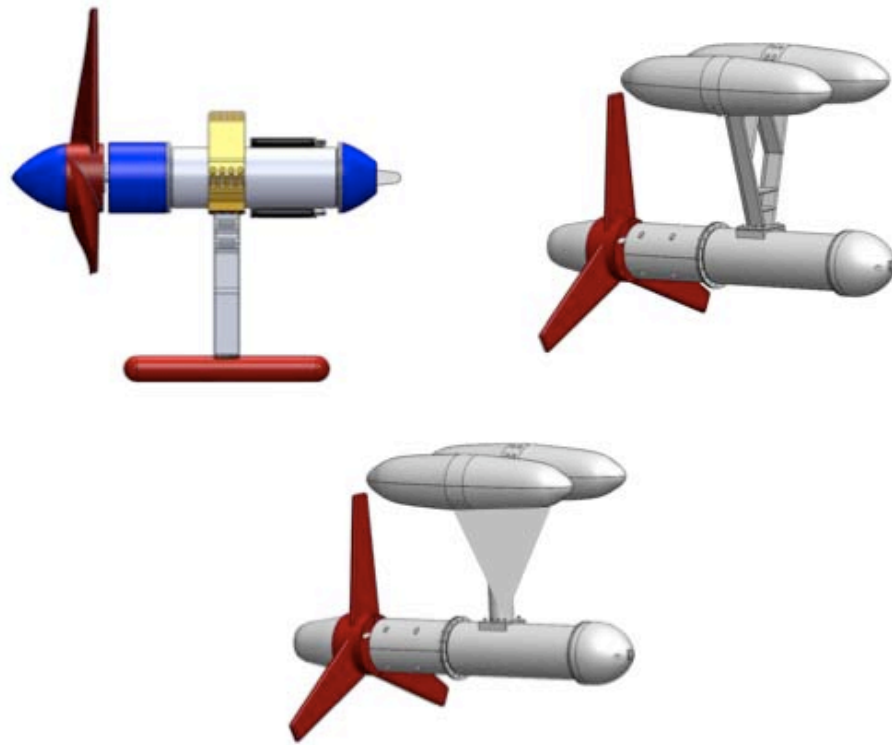
Figure 3 Two original designs of the OCTT on the top and the simplified turbine on the bottom.
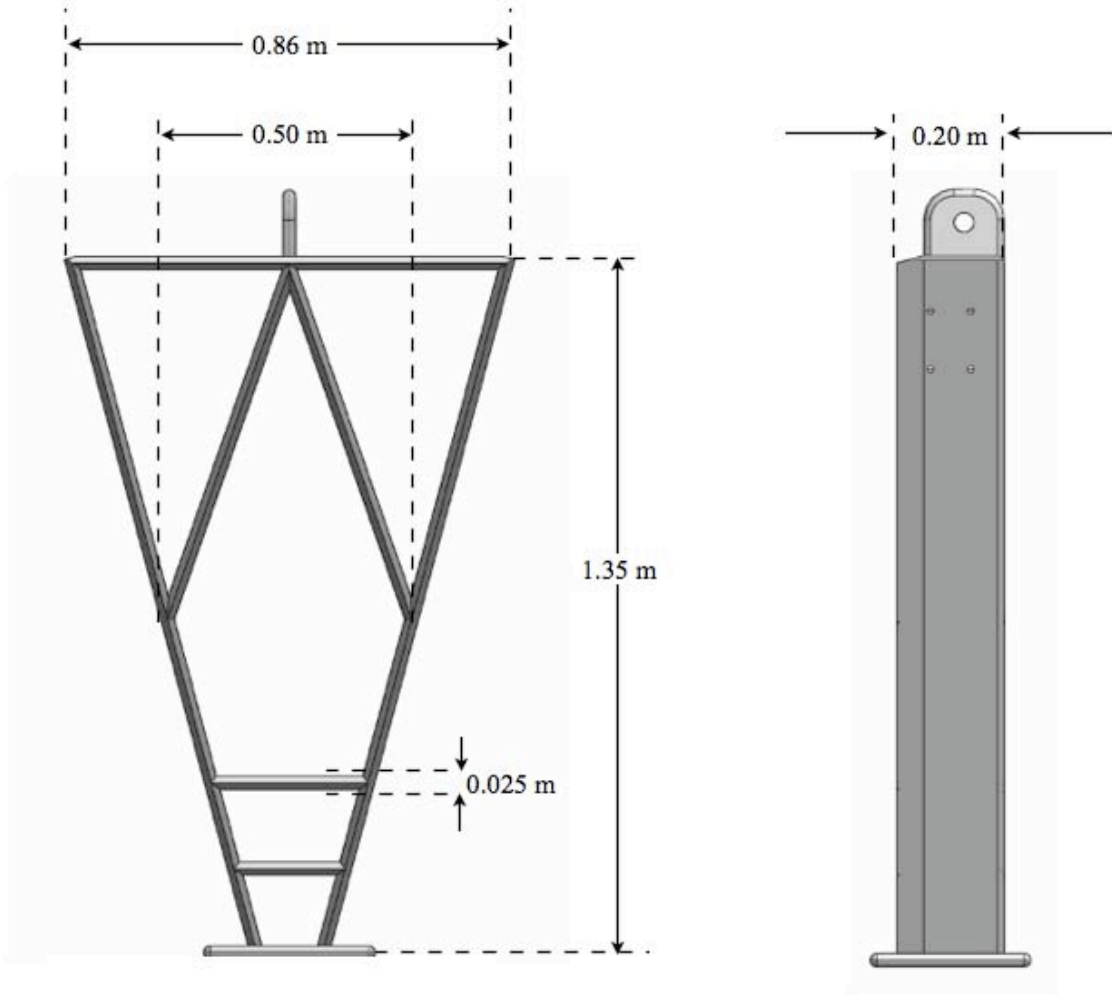
Figure 4 Trussed mast dimensions
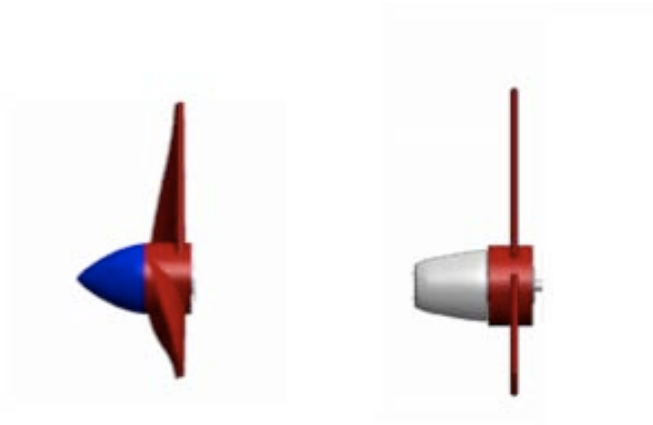
Figure 5 Description of the original (left) and idealized (right) rotor blades
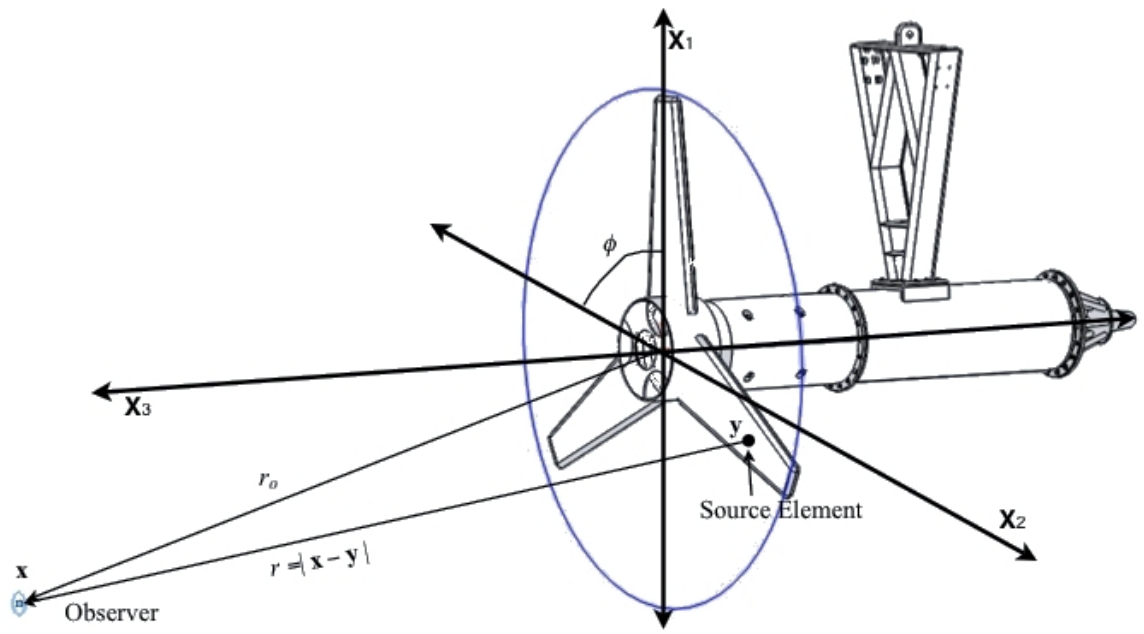
Figure 6 Coordinate system used in the calculations
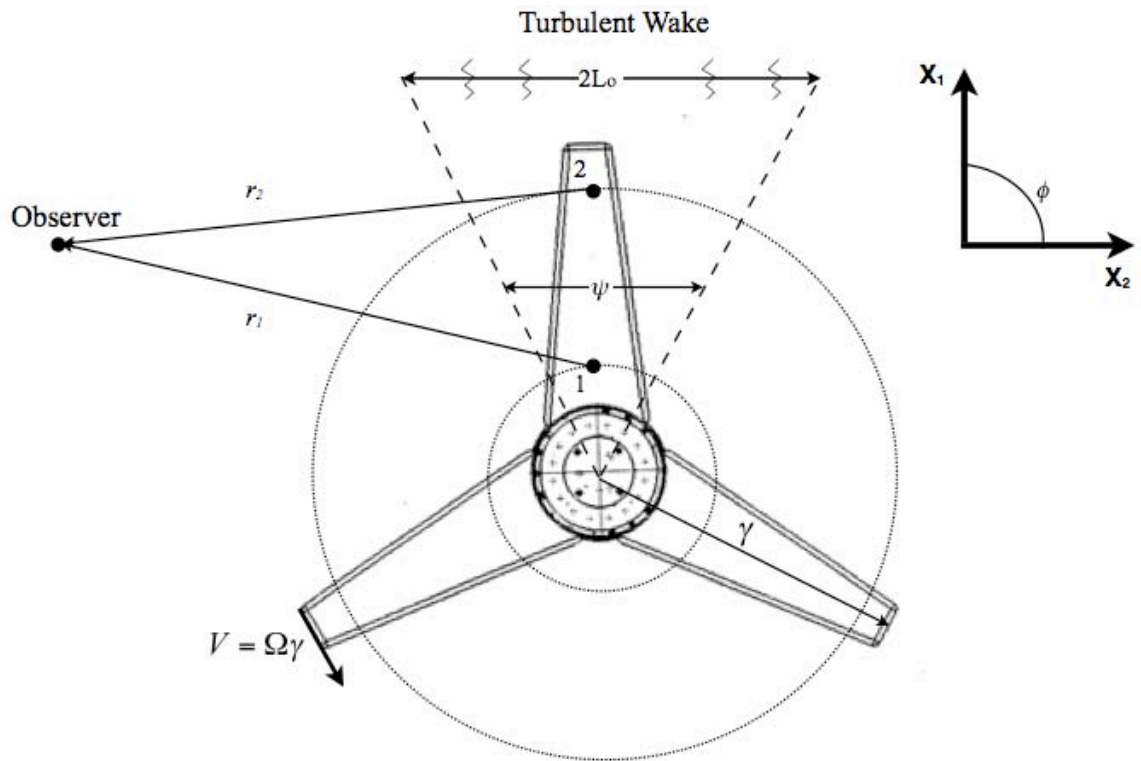
Figure 7 Front view representations of the point sources and the presence of the turbulent wake on the circular path (the length of L_o is exaggerated for illustration purposes)
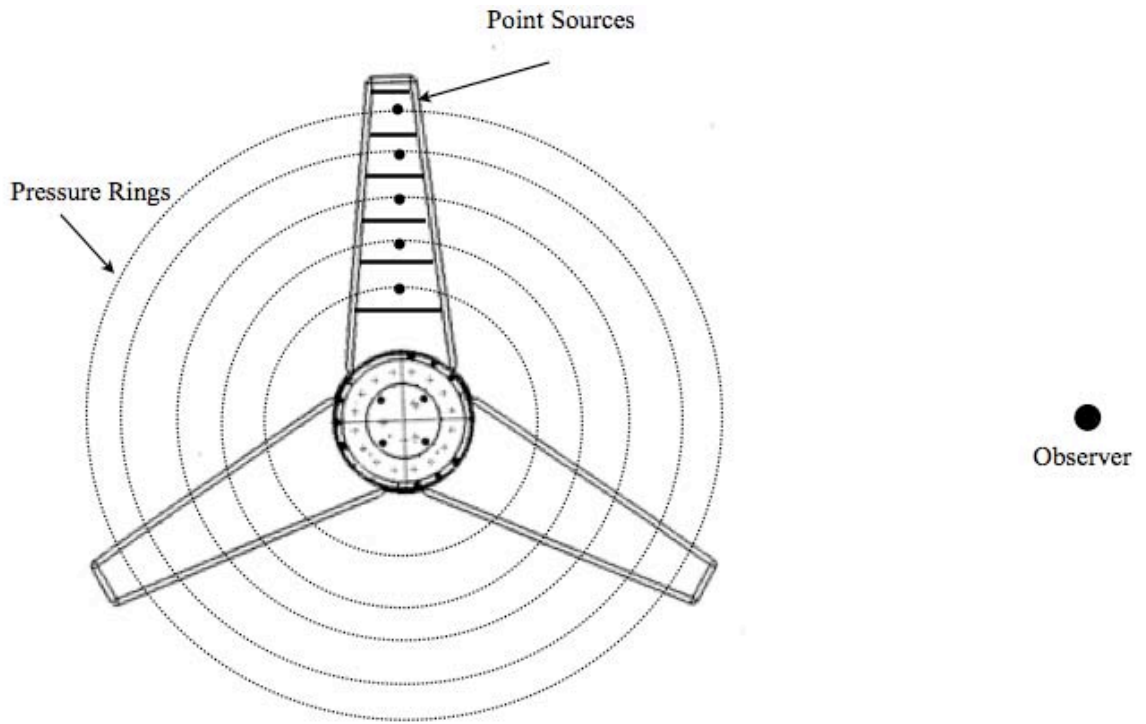
Figure 8 Representation of the different pressure rings formed by each of the point sources or blade sections
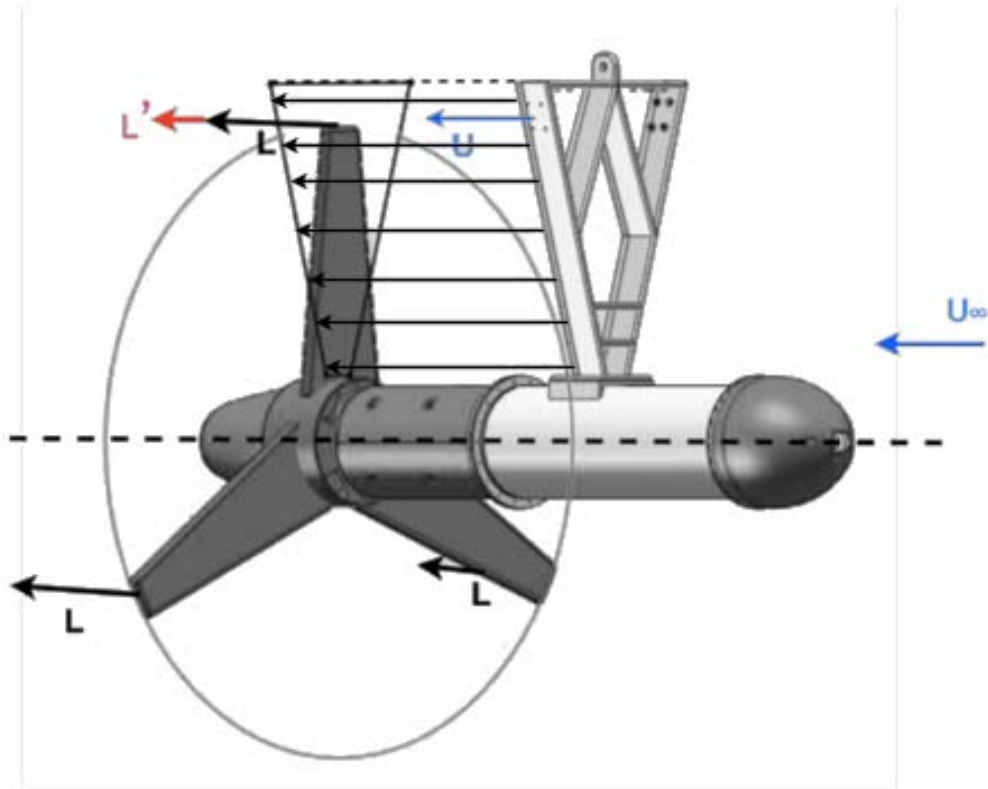
Figure 9 Illustration of the different regions where velocities change. *U* velocity occurs only within the triangular region or wake region whereas U_∞ occurs everywhere else. Representation of the changes in the lift L as it passes the through the different velocity profiles.
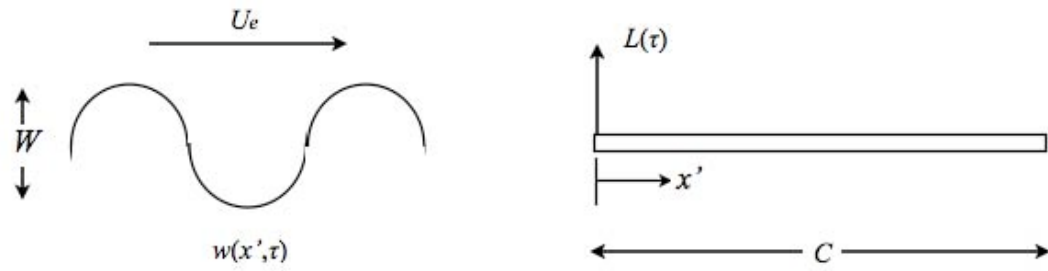
Figure 10 Idealized representation of a gust passing though a flat plate
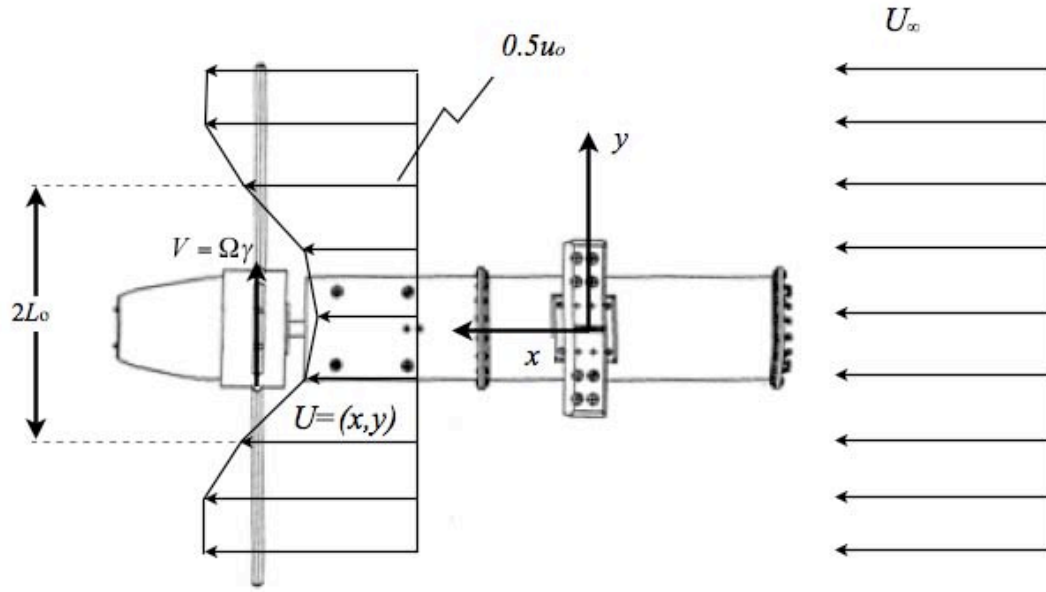
Figure 11 Tip passing through velocity profile on the wake region (top view). It can be seen in this figure how the velocity profile of U changes as it passes through the wake region
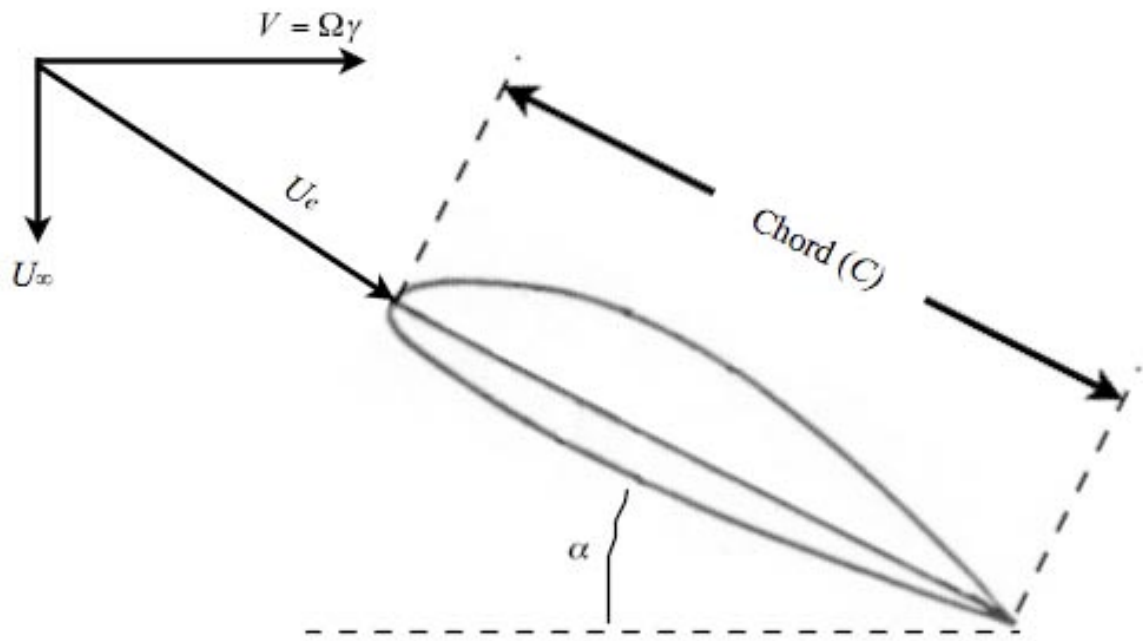
Figure 12 Idealized view of the incoming velocity at the leading edge as the blade travels everywhere around the circular except in the wake region
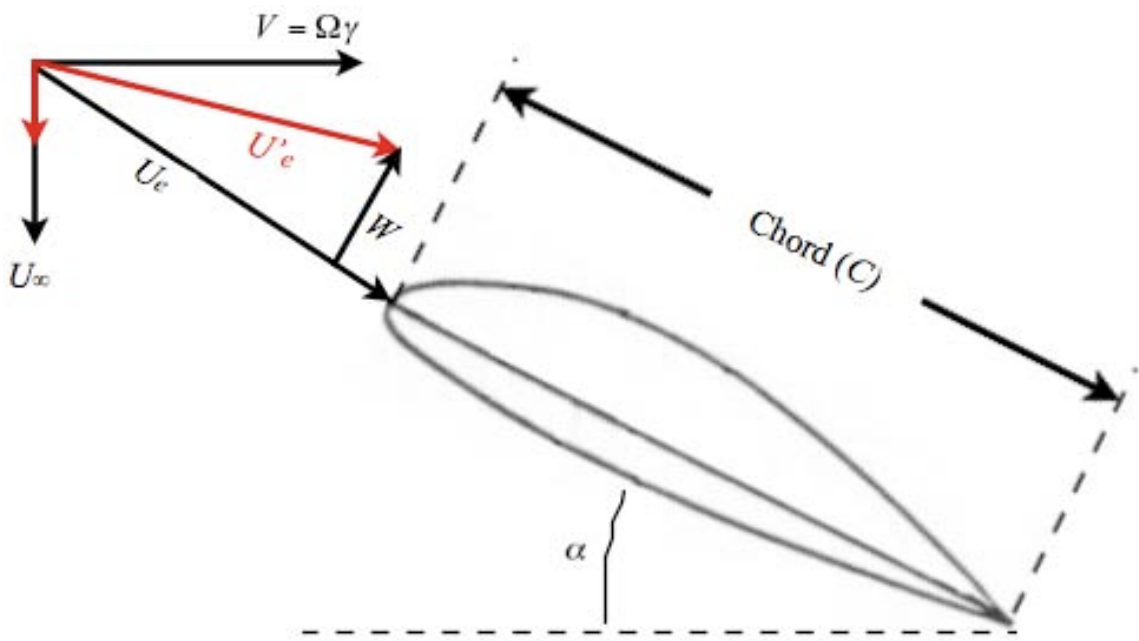
Figure 13 Idealized view of the incoming velocity at the leading edge as the blade travels through the wake region
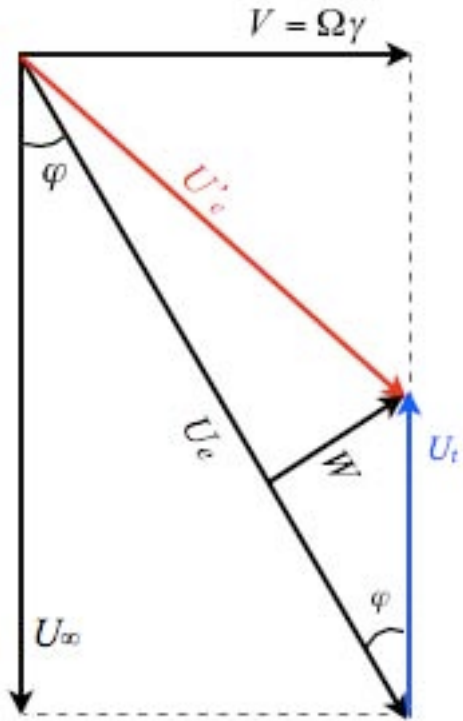
Figure 14 Vector diagram showing the geometrical relation between the different velocities
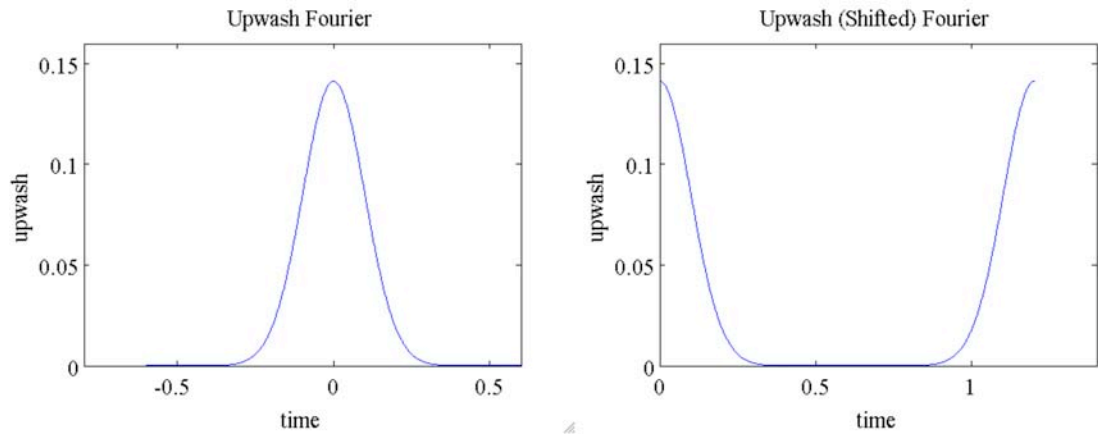
Figure 15 Graph of the general form of the upwash as a function of time
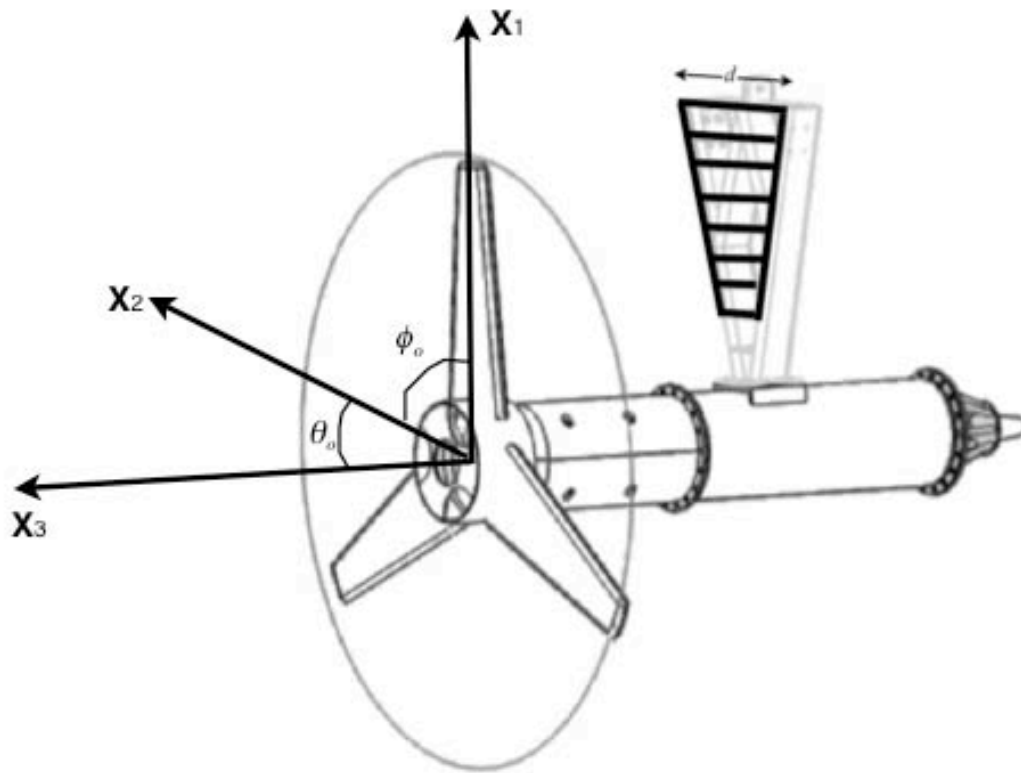
Figure 16 Simplified turbine, showing mast dimensions *C'* and *d*
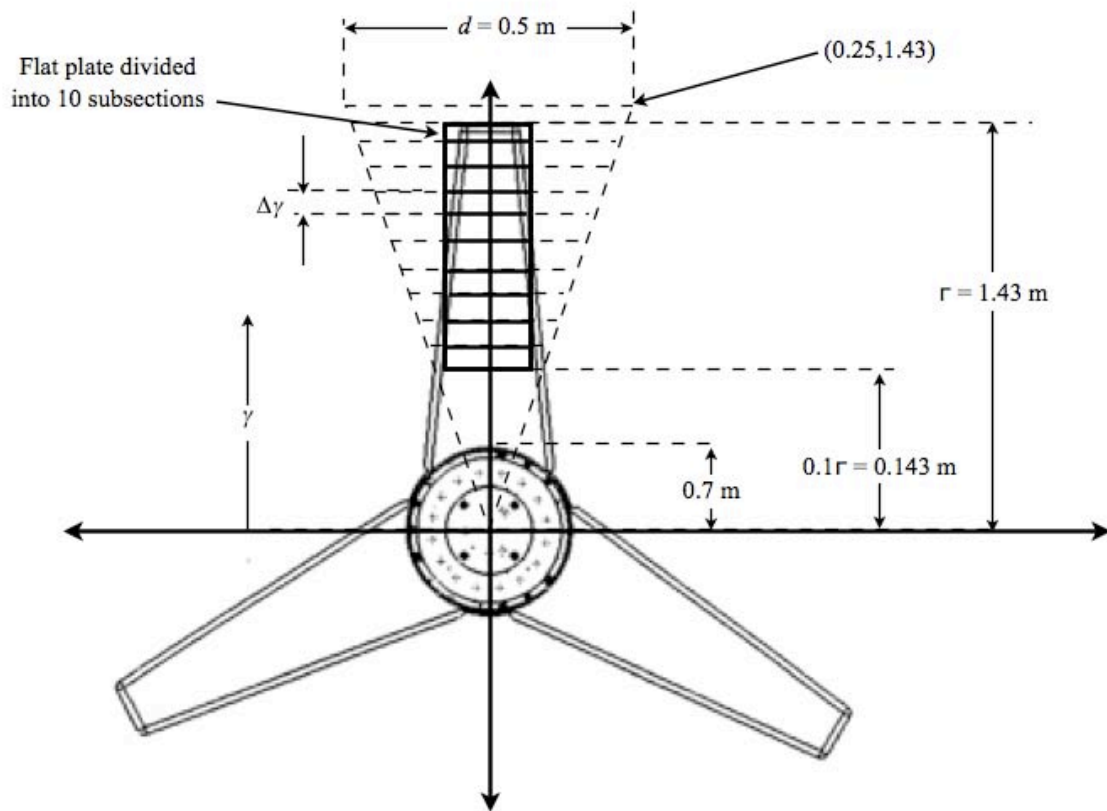
Figure 17 Sectioning from 10% of radius of the blade to its tip into a *B* number of subsections
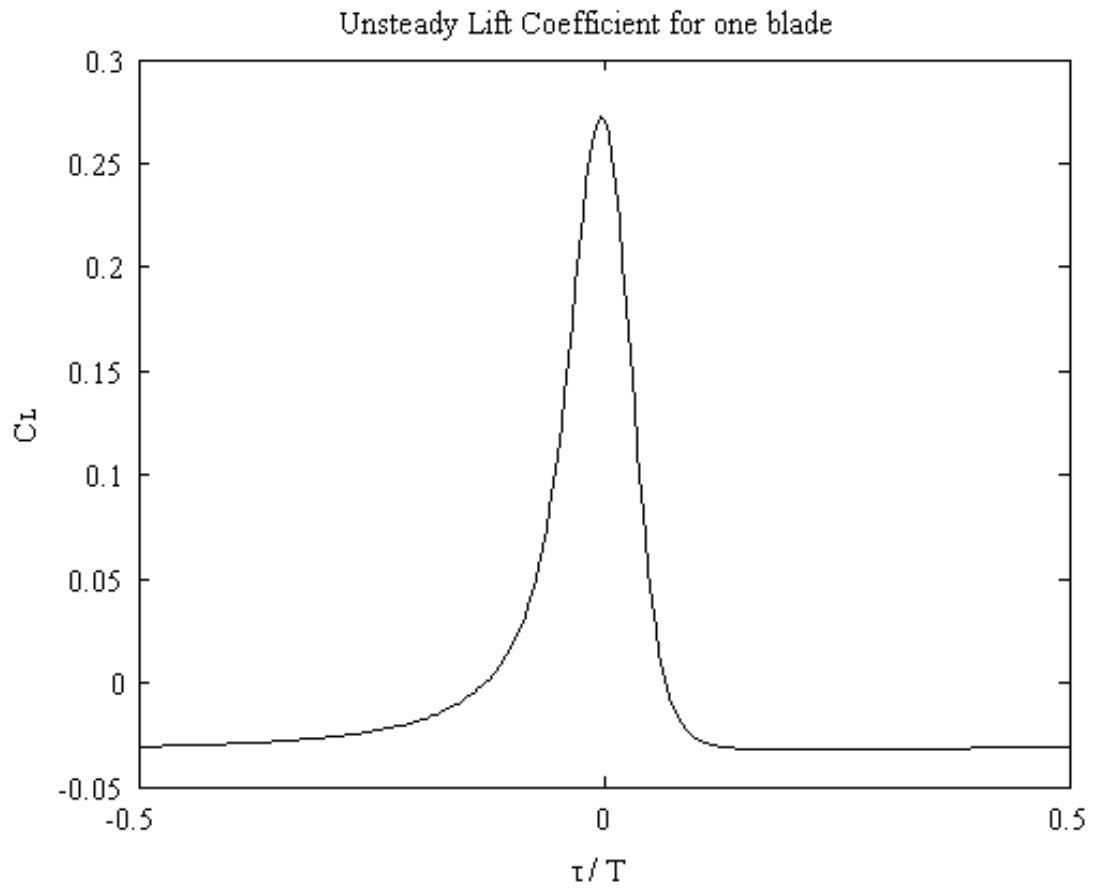
Figure 18 Unsteady Lift Coefficient for one blade, plotted against emission time t
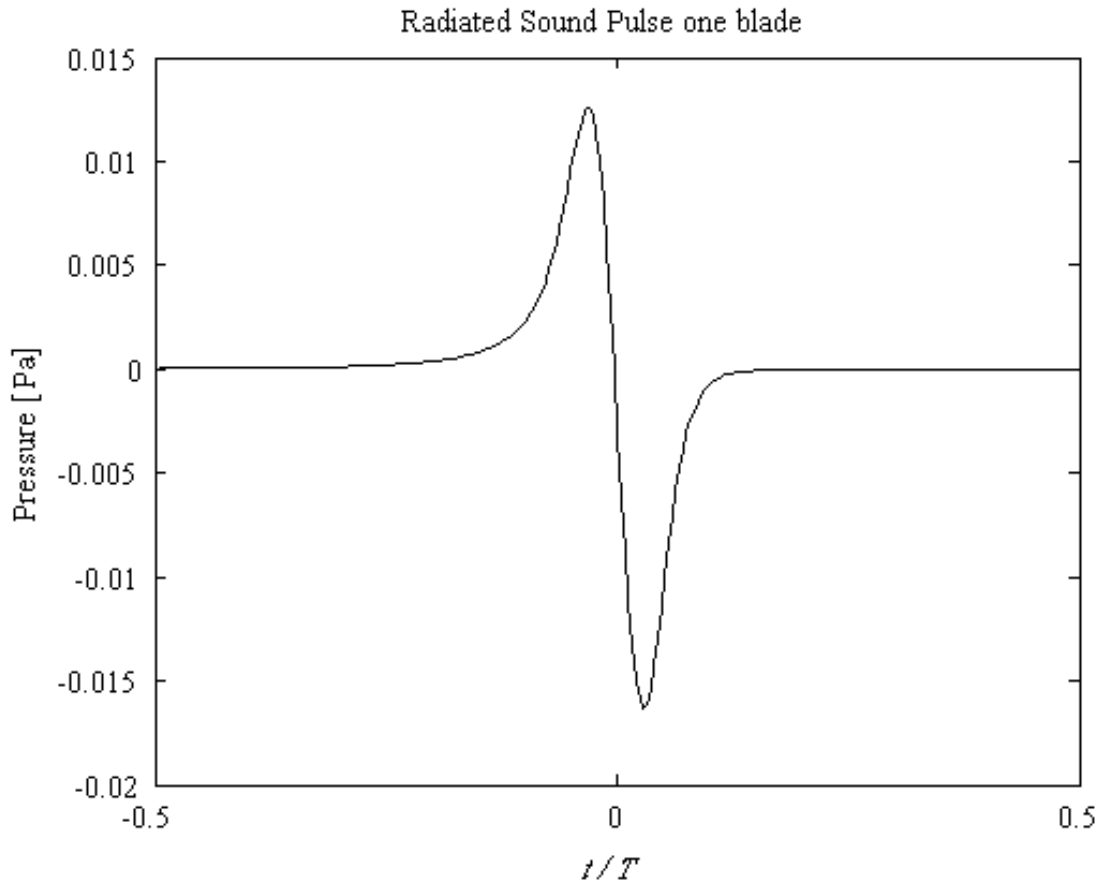
Figure 19 Time history of the radiated acoustic pressure generated by the simplified turbine, plotted against observer's time t over period T. Measured at an observer's location of spherical coordinates (100 m, 45º, 45º)
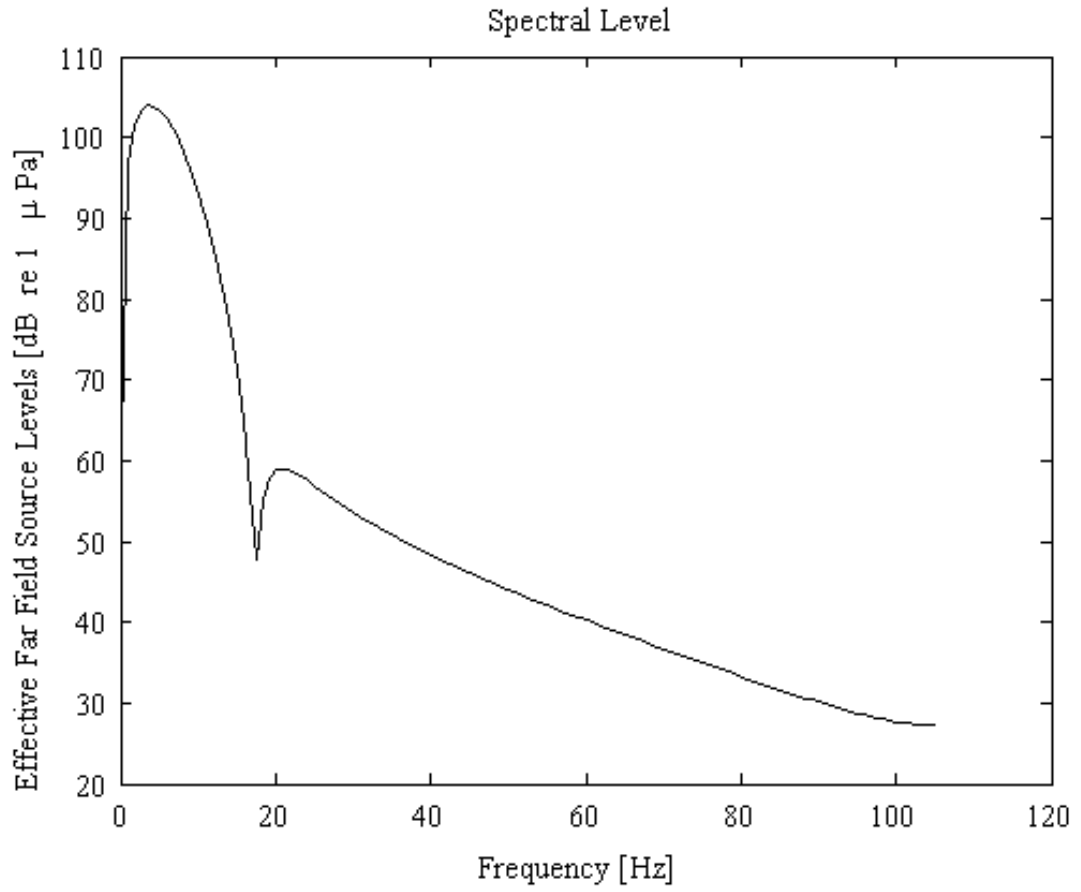
Figure 20 Noise levels felt at a point of observation positioned at spherical coordinates (100 m, 45º, 45º)
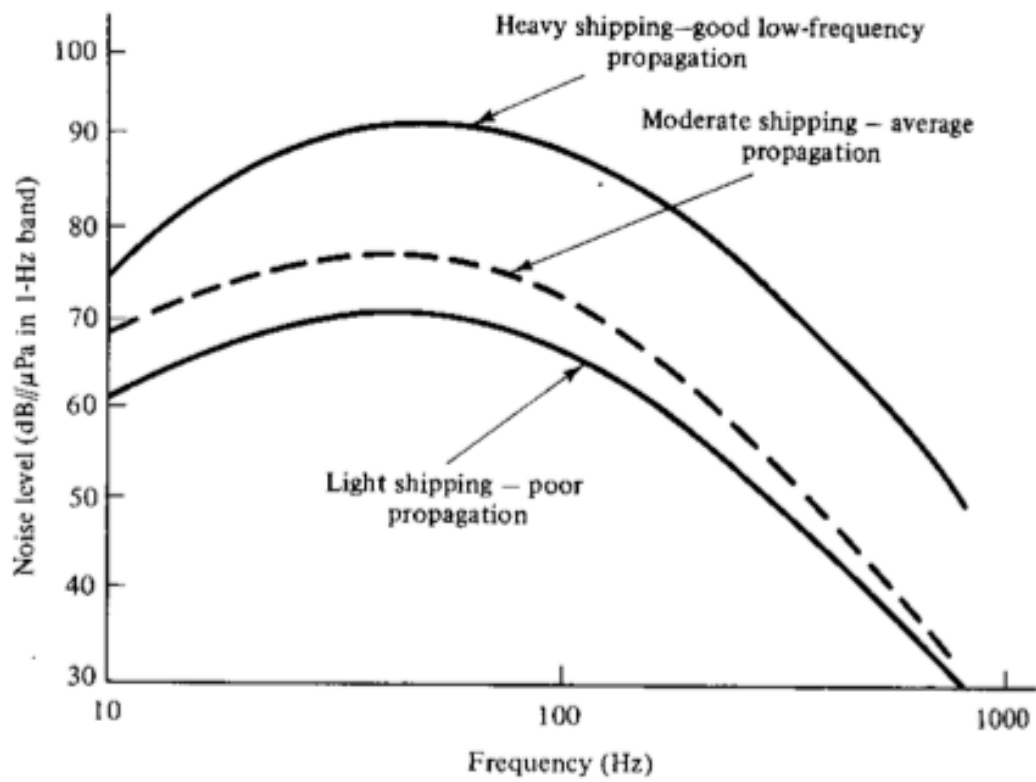
Figure 21 Distant shipping ambient noise levels [12]
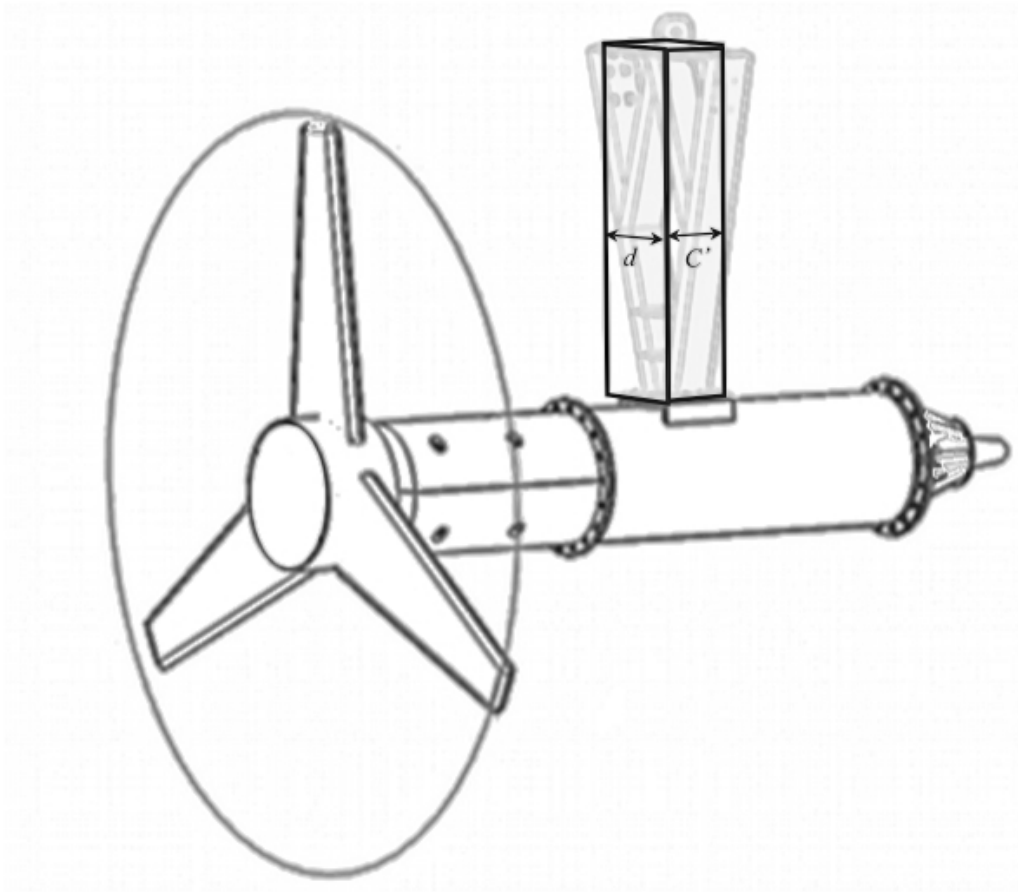
Figure 22 Depiction of the width of the structure kept uniformed in the span-wise direction
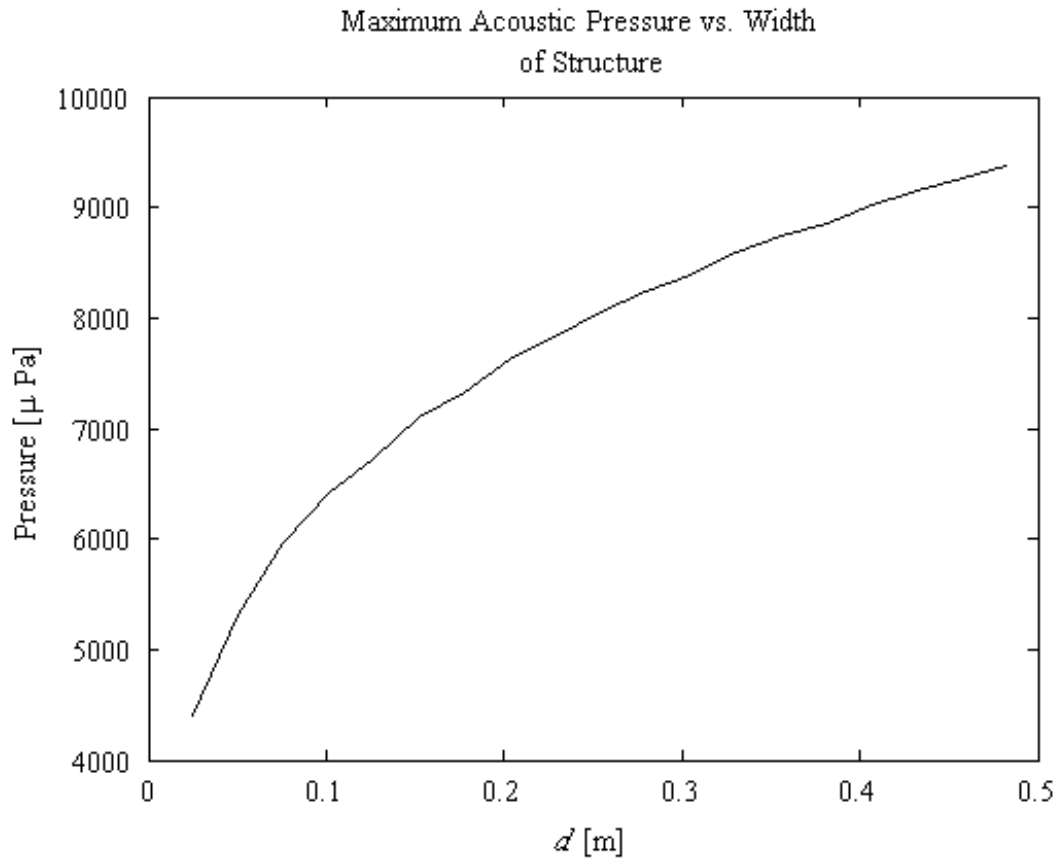
Figure 23 Plot of the maximum pressure vs. Width, for an observer positioned at (100 m, 45°, 45°)
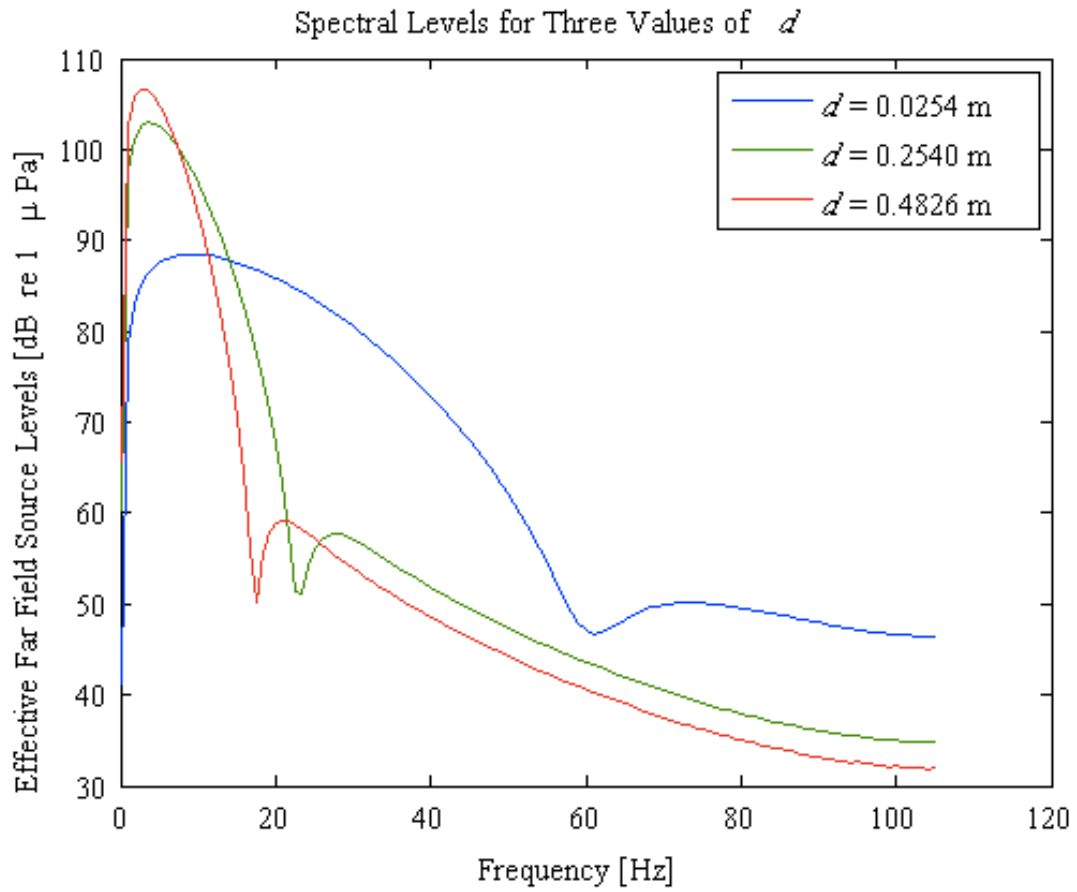
Figure 24 The noise levels for three different widths (0.0254 m, 0.254 m and 0.4826 m)
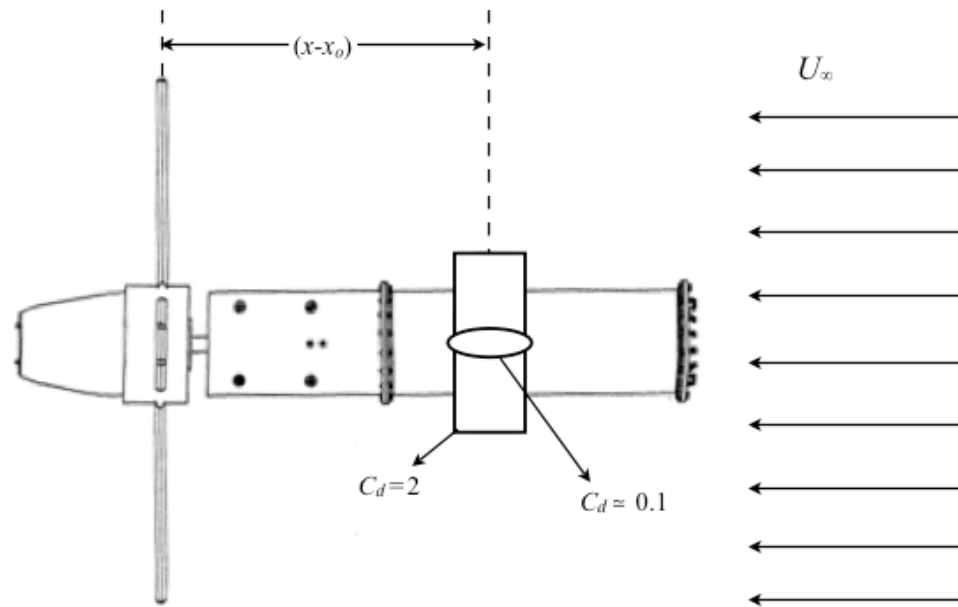
Figure 25 Depiction of cross-sectional shapes of the mast with their drag coefficients. Also depiction of the structure-blades distance $(x\text{-}x_o)$
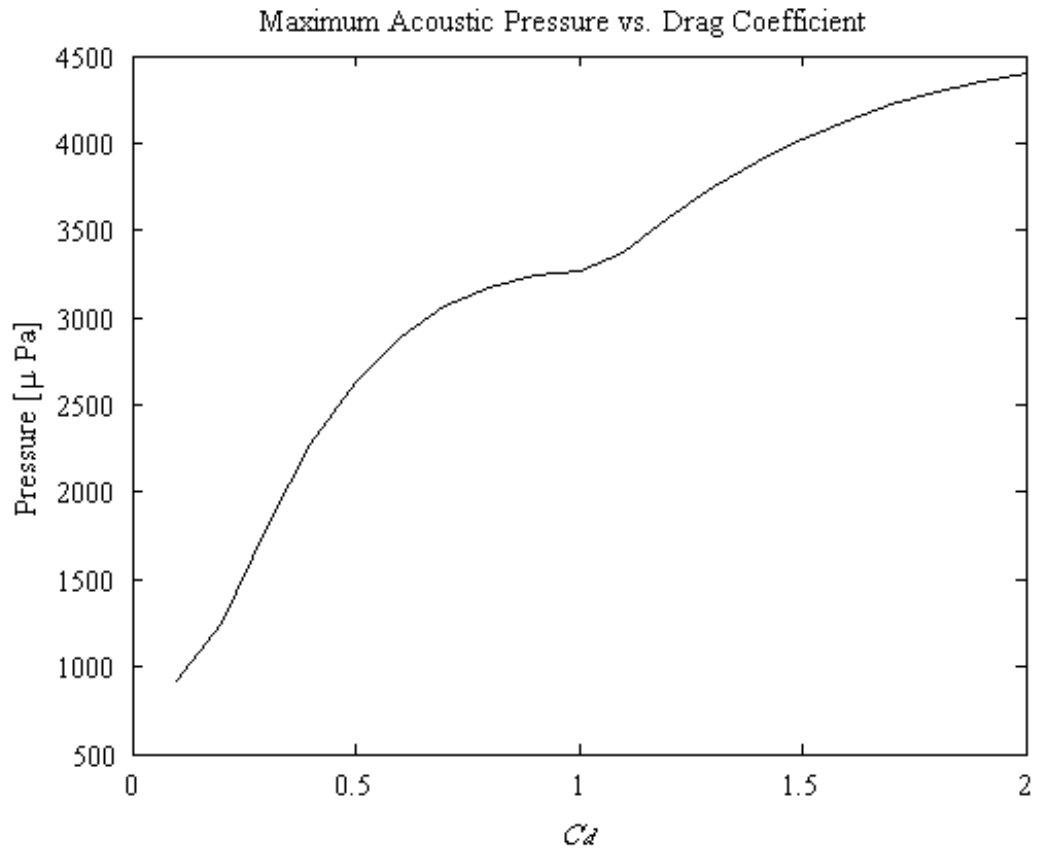
Figure 26 Plot of the maximum pressure vs. C_d, for an observer positioned at (100 m, 0º, 0º)
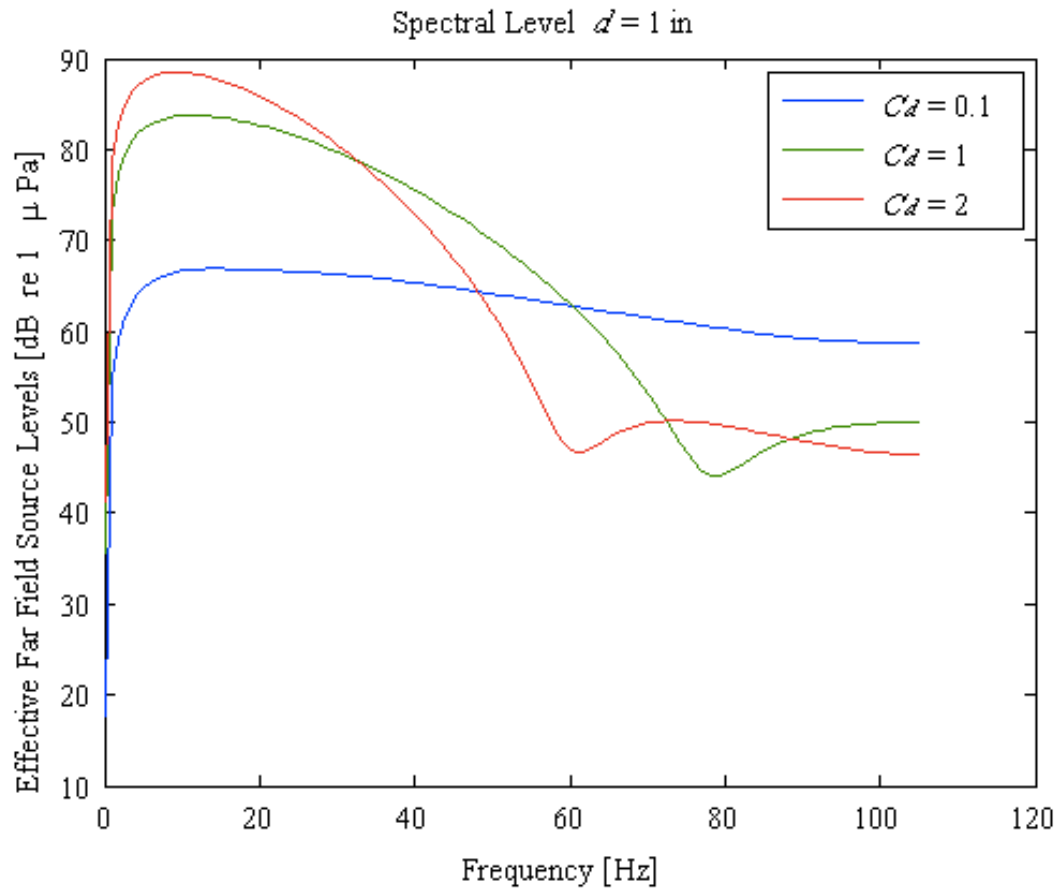
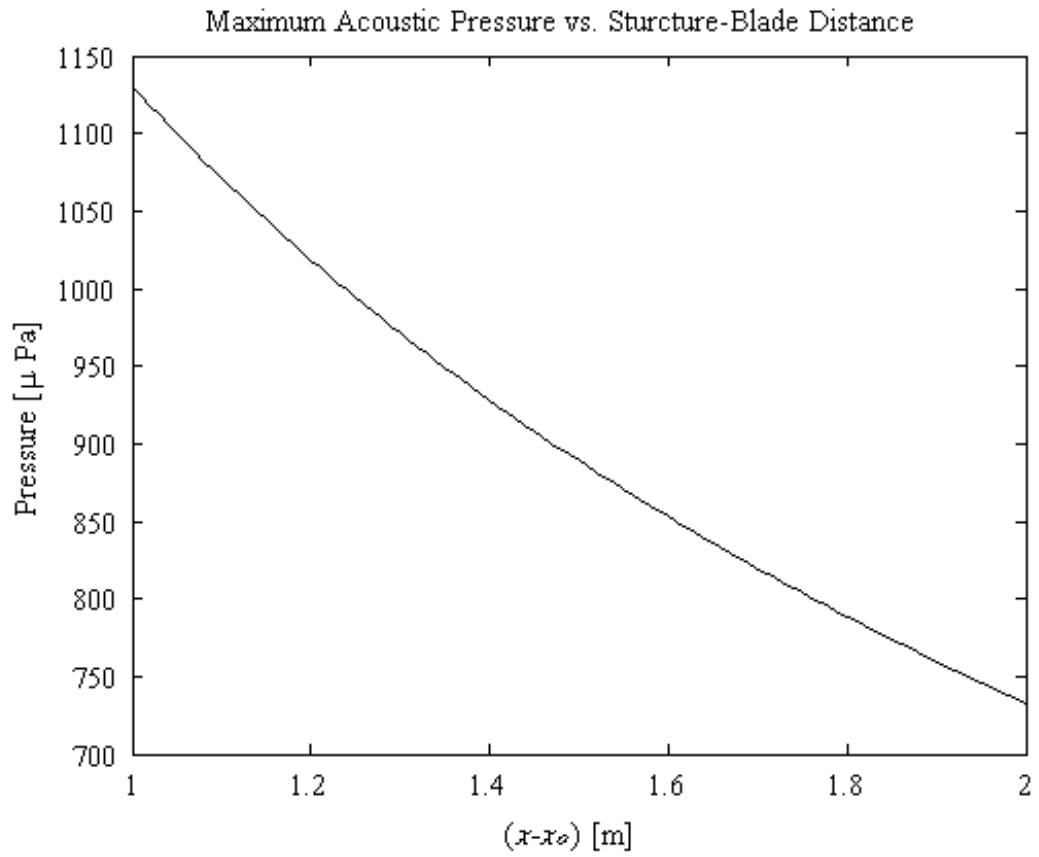Figure 27 The noise levels for three cross sectional shapes of different drag coefficients (C_d = 0.1, 1, 2)

Figure 28 Plot of the maximum pressure vs. structure-blade distance (x-x_o), for an observer positioned at (100 m, 0°, 0°)
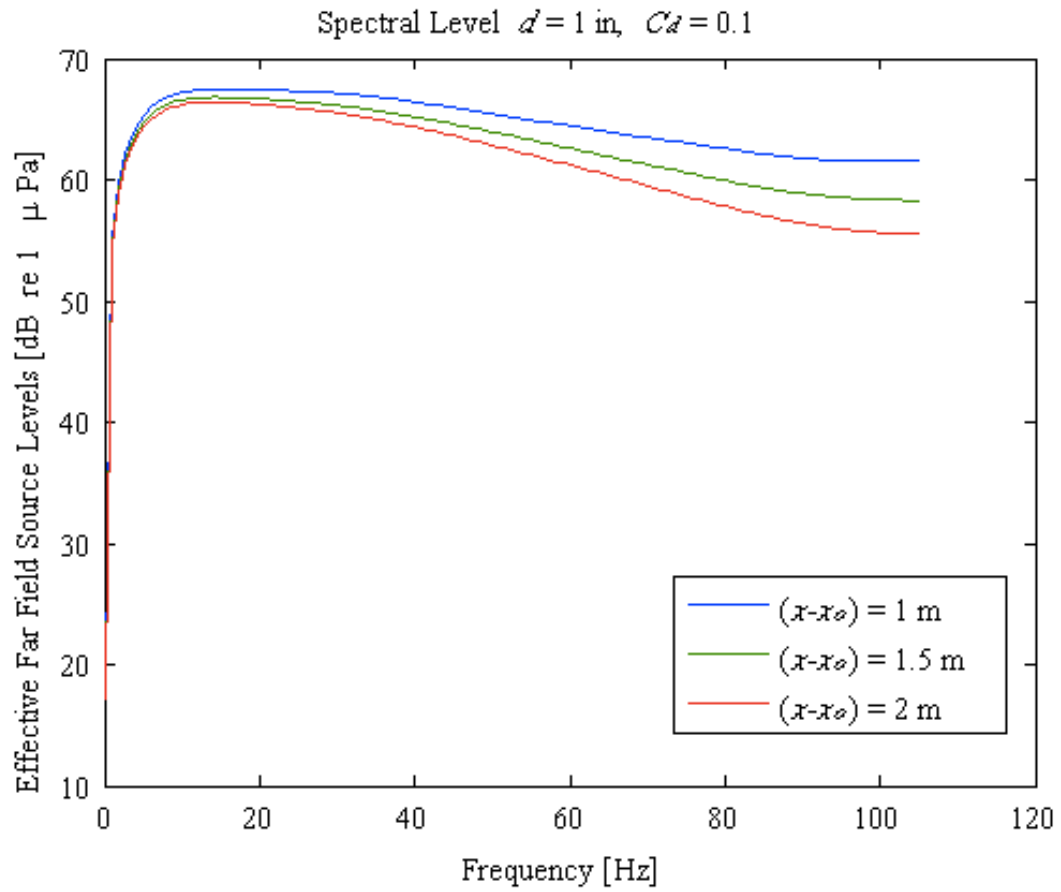
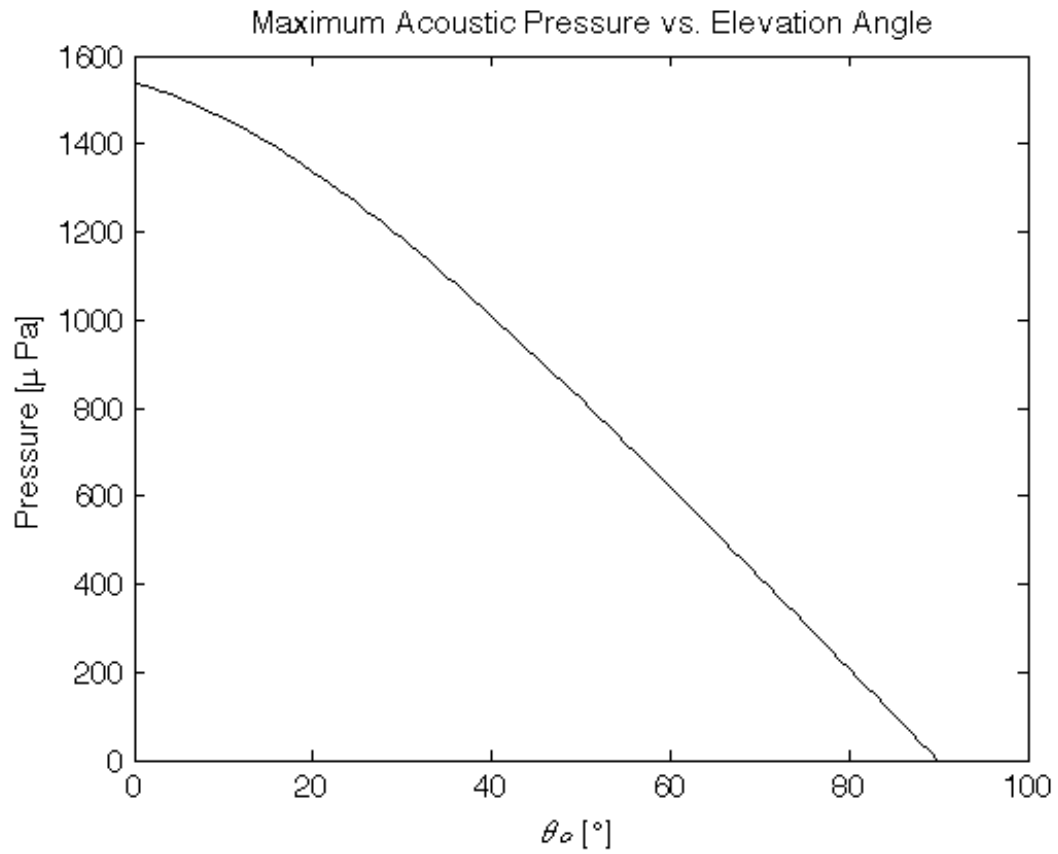Figure 29 The noise levels for three different structure-blade distances ($(x\text{-}x_o)$ = 0.1 m, 1 m, 2 m)

Figure 30 Plot of the maximum pressure vs. Elevation angle, for an observer positioned at (100 m, ϕ_o, 45°)
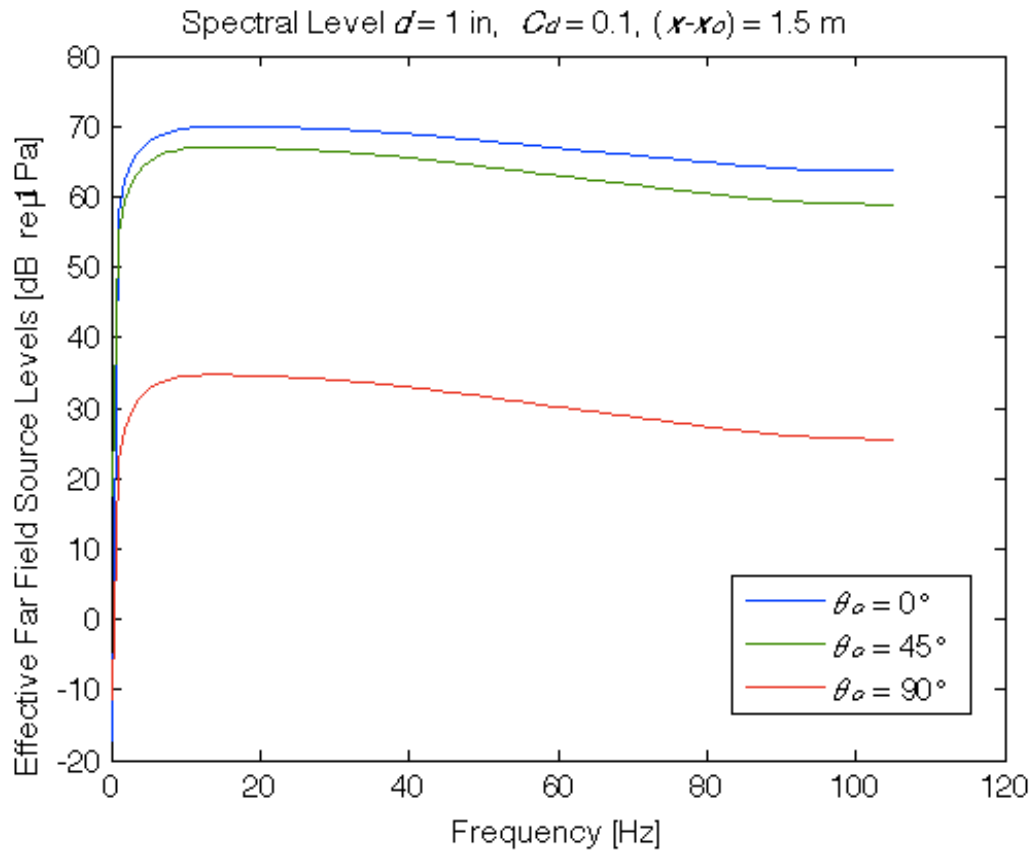
Figure 30 Plot of the maximum pressure vs. Elevation angle, for an observer positioned at (100 m, ϕ_o, 45°)

References

1. Daniel J. Alberts (2006), Lawrence Technological University. Addressing Wind Turbine Noise (pp. 8-9), International Marine.

2. James VanZwieten (2011), Technical Note: 40 vs. 50 RPM

3. Carlton. J. S (2007), Marine Propellers and Propulsion. Propeller Noise (pp. 253-259)

4. H. Seol, B. Jung, J. –C. Suh and S. Lee, Prediction of Non-Cavitating Underwater Propeller Noise. Journal of Sound and Vibration 257(1), 131-156

5. S Glegg, The Fundamentals of Aero and Hydroacoustics, Basic Concepts (pp. 41–53), Propeller and Rotor Noise (pp. 1-37)

6. S. Glegg, 1983 Noise and Vibration, Fan Noise (pp. 440-450). R.G White and J. Walker, Ellis Horwood

7. W.R. Sears, Some aspects of non-stationary airfoil theory and its practical applications, Journal of the Aeronautical Sciences 8 (1941) 104–108

8. A 20 KW Open Ocean Current Test Turbine

9. J. N. Newman (1997), Marine Hydrodynamics. Lifting Surfaces (pp. 160-168)

10. S. Glegg and William Devenport (2008), Journal of Sound and Vibration. Volume 319 issues 3-5, Unsteady Loading on an Airfoil of Arbitrary Thickness (pp 1252-1258).

11. I. Wygnanski, F. Champagne and B. Marasli (1986), Journal of Fluid Mechanics, vol. 168, On the Large-scale Structures in Two-dimensional Small-deficit, Turbulent wakes (pp. 31-71)

12. William S. Burdic (1984), Underwater Acoustic System Analysis. Fourier Methods (pp. 158-168)